Stem Cell Reports
Article
ISSCR
OPEN ACCESS

MFN2 Plays a Distinct Role from MFN1 in Regulating Spermatogonial Differentiation

Wei Chen,[1] Yun Sun,[1] Qi Sun,[1] Jingjing Zhang,[2] Manxi Jiang,[3] Chingwen Chang,[4] Xiaoli Huang,[1] Chuanyun Wang,[1] Pengxiang Wang,[1] Zhaoran Zhang,[4] Xuejin Chen,[3] and Yuan Wang[4,*]

[1]Shanghai Key Laboratory of Regulatory Biology, Institute of Biomedical Sciences and School of Life Sciences, East China Normal University, Shanghai 200241, China

[2]Translational Medicine Research Center, Affiliated Hangzhou First People's Hospital, Zhejiang University School of Medicine, Hangzhou 310006, China

[3]Department of Animal Science, School of Medicine, Shanghai JiaoTong University, Shanghai 200025, China

[4]Department of Animal Sciences, College of Agriculture and Natural Resources, Michigan State University, East Lansing, MI 48824, USA

*Correspondence: wangyu81@msu.edu

https://doi.org/10.1016/j.stemcr.2020.03.024

SUMMARY

Although mitochondrial morphology is well-known for its role in cellular homeostasis, there is surprisingly little knowledge on whether mitochondrial remodeling is required for postnatal germ cell development. In this study, we investigated the functions of MFN1 and MFN2, two GTPases in mitochondrial fusion, during early spermatogenesis. We observed increased MFN expressions along with increased mitochondrial and endoplasmic reticulum (ER) activities during spermatogonial differentiation. Deletion of either *Mfn* led to DNA oxidation and apoptosis specifically in differentiating spermatogonia and spermatocytes, which in turn caused male infertility. We further found MFN2 regulated spermatogenesis by modulating both mitochondrial and ER functions, a mechanism distinct from that of MFN1. Defects of germ cell development in MFN2 mutants were corrected by MFN2 at either mitochondria or ER but not by MFN1. Our study thus reveals an essential requirement of MFN-mediated mitochondrial and ER coordination in spermatogenesis, providing critical insights into mitochondrial determinants of male fertility.

INTRODUCTION

Mammalian postnatal male germ cell development is known as spermatogenesis, during which haploid spermatozoa are produced through stages of differentiation, meiosis, and maturation (Wylie, 1999). In this process, spermatogonial stem cells maintain a pool of undifferentiated progenitor spermatogonia which will further differentiate, in response to developmental cues, such as retinoic acid, and become KIT+ differentiating spermatogonia (Mecklenburg and Hermann, 2016; Wylie, 1999; Yang and Oatley, 2014). In mice, primary spermatocytes develop from differentiating type B spermatogonia and sequentially become secondary spermatocytes and haploid spermatids via two rounds of meiosis by postnatal day 21 (P21) in the first-wave spermatogenesis (Mecklenburg and Hermann, 2016; Yang and Oatley, 2014). These dramatic changes of germ cells during spermatogenesis, especially in the processes of spermatogonial differentiation and spermatocyte formation, require orchestrated actions of subcellular organelles.

Notably, the architecture and distribution of mitochondria differ in germ cells at different stages of spermatogenesis (Chuma et al., 2009; De Martino et al., 1979; Eddy, 1975). Although mitochondria with less dense matrix and more compact crista compartment exist in spermatogonia, pachytene spermatocytes contain mitochondria that are in a condensed form (Ramalho-Santos and Amaral, 2013). In addition, in spermatogonia and early-stage spermatocytes, perinuclear mitochondria cluster within a germ cell-specific subcellular structure, called intermitochondrial cement (IMC), where primary Piwi-interacting RNA (piRNA) biogenesis occurs (Grivna et al., 2006; Lau et al., 2006). The piRNAs are crucial for maintaining genome integrity of germ cells by inhibiting the expression of transposable elements (Grivna et al., 2006; Lau et al., 2006). However, underlying mechanisms how distinct mitochondrial features are maintained during early spermatogenesis and their developmental importance are yet to be defined.

Mitochondrial features are largely regulated by their fission and fusion, collectively known as mitochondrial dynamics (Chan, 2006). Through mitofusion (i.e., mitochondrial fusion) and fission, mitochondria continuously change between tubular and fragmented morphology, and in turn modify their architecture to respond to various environmental stimuli and cellular requirements (Chan, 2006). More importantly, mitochondrial dynamics ensure exchanging of mitochondrial contents, which allows coordinated responses of individual mitochondria to extracellular cues (Chan, 2006). Mitofusion is mainly regulated by two GTPases, mitofusin 1 (MFN1) and mitofusin 2 (MFN2) (Chen et al., 2003; Santel et al., 2003). Additional factors, such as MitoPLD, also contribute to mitofusion in an MFN1- and MFN2-dependent manner (Huang et al., 2011; Watanabe et al., 2011). Null mutation of *MitoPLD* in mice leads to mislocalized mitochondria to centrosomes, lack of IMC formation, reduced piRNA

biosynthesis, and altered expression of transposable elements, which in turn result in male infertility (Huang et al., 2011; Watanabe et al., 2011). *Mfn1* conditional deletion from germ cells also causes male infertility (Zhang et al., 2016). However, IMC remainsintact in *Mfn1* knockout mice without alteration in the expression of transposable elements (Zhang et al., 2016), thereby supporting distinct functional mechanisms of different pro-mitofusion molecules in regulating spermatogenesis. It has yet to be fully ascertained how MFN-dependent mitochondrial activities contribute to postnatal germ cell development.

Mitochondrial functions are also regulated by their interaction with other subcellular organelles, including endoplasmic reticulum (ER) (de Brito and Scorrano, 2008). In addition to its roles in protein synthesis, folding, and transport, ER is also the storage site for Ca^{2+}, which is released upon stimulation (Rizzuto et al., 1998). Disturbed ER homeostasis induces ER stress, characterized by Ca^{2+} release from ER into cytoplasm and a surge of unfolded or misfolded proteins (Bukau et al., 2006; Gaut and Hendershot, 1993). This in turn leads to increased expression of ER chaperon proteins to restore ER homeostasis (Bukau et al., 2006; Gaut and Hendershot, 1993). Increased cytosolic Ca^{2+} may disturb Ca^{2+} signaling, upregulate mitochondrial Ca^{2+} load, and trigger cell death (Bukau et al., 2006; Gaut and Hendershot, 1993; Rizzuto et al., 1998). Moreover, ER membrane connects dynamically to mitochondria and may regulate mitochondrial Ca^{2+} levels by modulating mitochondrion-ER juxtaposition (de Brito and Scorrano, 2008; Rizzuto et al., 1998; Schneeberger et al., 2013). Currently, it is unclear whether the state of ER contributes to postnatal germ cell development, nor do we know how ER homeostasis is regulated during spermatogenesis.

MFN1 and MFN2 are ubiquitously expressed, but their expression levels and exact functions in regulating mitochondrial and ER activities depend upon specific cell types (Chen et al., 2007; de Brito and Scorrano, 2008; Dietrich et al., 2013; Santel et al., 2003; Schneeberger et al., 2013). We previously demonstrated that GASZ, a germ cell-specific protein, also known as ASZ1 (Ma et al., 2009), interacted with both MFN1 and MFN2 in testes, suggesting an intrinsic contribution of MFN-mediated functions to spermatogenesis (Zhang et al., 2016). To understand the functional importance and underlying mechanisms of mitochondrial and ER functions in postnatal germ cell development, we hereby investigated the roles of MFN1 and MFN2 during spermatogenesis using conditional *Mfn* knockout mice. Intriguingly, we found that MFN1 and MFN2 affected spermatogenesis in distinct manners. In neonatal pro-spermatogonia, only MFN1 regulated mitochondrial fusion. Later in spermatogenesis, loss of MFN2 notably impaired both mitochondrial functions and increased ER stress. Nevertheless, both MFN1 and MFN2 are required for sustaining spermatogonial differentiation and spermatocyte formation during early spermatogenesis. Our study thus reveals an essential need for MFN-mediated mitofusion and ER homeostasis in sustaining male fertility.

RESULTS

Elevated Mitochondrial and ER Activities during Spermatogonial Differentiation

Cellular reactive oxygen species (ROS) is largely produced from mitochondrial respiration (Dickinson and Chang, 2011), while the ER is the major Ca^{2+} storage site (Rizzuto et al., 1998) for maintaining a proper cytoplasmic Ca^{2+} level. To understand changes in mitochondrial and ER activities during early spermatogenesis, we first examined the ROS and Ca^{2+} levels from CD90+/KIT− undifferentiated spermatogonia and KIT+ differentiating spermatogonia from mice at P12. At this stage, only differentiating spermatogonia and primary spermatocytes before the pachytene stage are formed (Figure S1A). We observed that both cytoplasmic ROS and Ca^{2+} levels were significantly upregulated in KIT+ cells (Figures 1A and 1B). In addition, the expression levels of ER chaperon proteins were also increased (Figure 1C), indicating elevated activities of both mitochondria and ER.

Because MFNs (i.e., MFN1 and MFN2) are key regulators of mitochondrial dynamics, we further examined their expression at various stages during spermatogenesis. Interestingly, we found that protein levels of MFN1 and MFN2 increased between P7 and P14, a period during which spermatogonial differentiation and meiosis I start (Figures 1D and S1A). In addition, we examined *Mfn1* and *Mfn2* expression in sorted CD9+/KIT− undifferentiated spermatogonia and the KIT+ population by real-time RT-PCR. We found comparable transcript levels between *Mfn1* and *Mfn2*, but for both MFNs the expression levels were higher in KIT+ cells than those in CD9+/KIT− undifferentiated spermatogonia (Figure 1E). These data thus suggest that high levels of MFNs are required for proper spermatogonial differentiation and primary spermatocyte formation.

MFN Deficiency Affects Spermatogonial Differentiation and Spermatocyte Formation

We previously demonstrated that the germline protein GASZ was localized to mitochondrial outer membrane and interacted with both MFN1 and MFN2 to regulate mitochondrial functions (Zhang et al., 2016). In addition, *Mfn1* conditional knockout in germ cells resulted in male

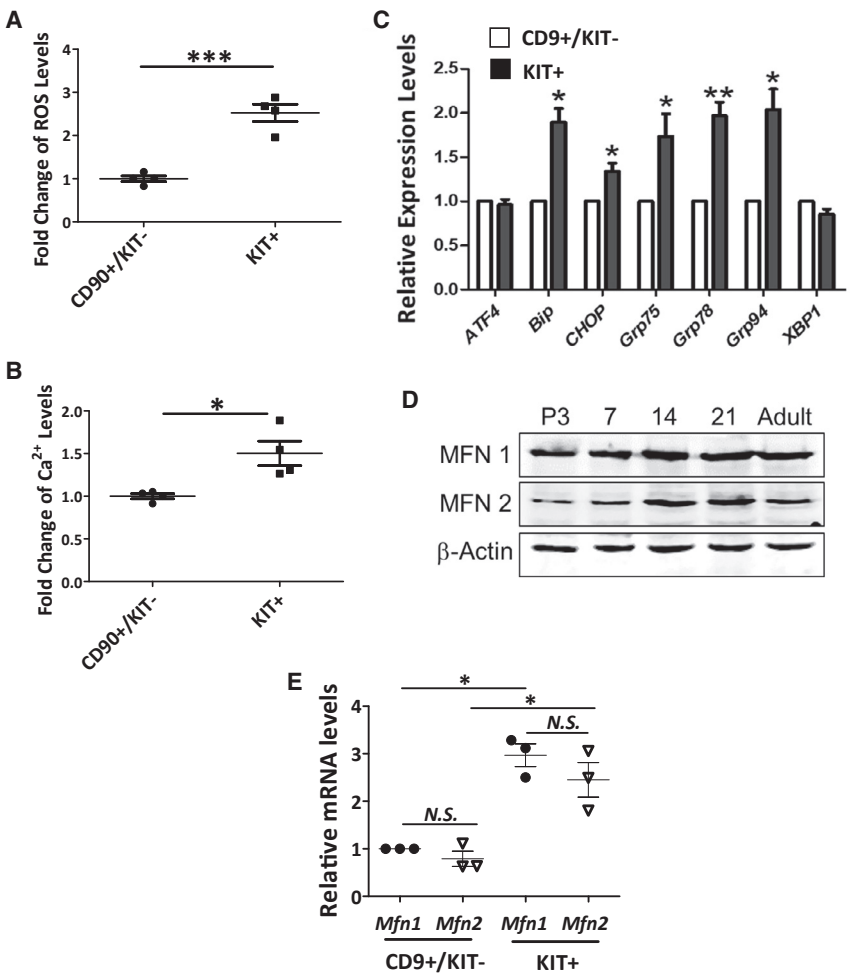

Figure 1. Elevated Mitochondrial/ER Activities and MFN Expression during Spermatogonial Development

(A and B) ROS (A) and cellular Ca^{2+} levels (B) were measured in CD90+/KIT− undifferentiated spermatogonia and KIT+ differentiating spermatogonia collected from wild-type P12 testes by flow cytometry.

(C) Real-time RT-PCR analyses on the expression of ER chaperons in sorted CD9+/KIT− undifferentiated spermatogonia and KIT+ differentiating population from wild-type P12 testes.

(D) Protein levels of MFN1 and MFN2 were measured by western blots in testes collected at various time points during spermatogenesis.

(E) Real-time RT-PCR analyses on *Mfn1* and *Mfn2* expression in sorted CD9+/KIT− and KIT+ cells from wild-type P12 testes.

(A–C and E) Data are presented as mean ± 1 SEM from three or more biological replicates. Fold changes or expression levels were compared with mean value of CD90+/KIT− or CD9+/KIT− cells. *p < 0.05, **p < 0.01, ***p < 0.001; N.S., no statistical significance.

infertility (Zhang et al., 2016). To understand whether MFN2 also regulates spermatogenesis, we crossed a *Mfn2* conditional knockout mice with a *Ddx4-Cre* line, in which Cre recombinase under the germ cell-specific promoter of *Ddx4* (Gallardo et al., 2007) deletes *Mfn2* in gonocytes at 15.5 days post coitum (Figures S1A and S1B). Compared with their littermate controls, *Mfn2* conditional knockout (*Mfn2$^{f/f}$; Ddx4-Cre,* abbreviated as *Mfn2 CKO* in figures) testes were smaller at P14 (Figure 2A) and were dramatically reduced in size at adulthood (Figure S1D). Histology examination at various time points during spermatogenesis revealed that germ cell formation started to reduce in *Mfn2$^{f/f}$; Ddx4-Cre* testes at P10, with much fewer spermatocytes at P14 (Figure 2B). No spermatids were detected in MFN2-deficient testes at week 5 or later (Figure 2B). These data support an essential requirement of MFN2 for sustaining male fertility.

Interestingly, cells positive for DDX4, the germ cell maker, only existed along the base of seminiferous epithelium in *Mfn2$^{f/f}$; Ddx4-Cre* testes (Figure 2C). By contrast, in littermate controls, high DDX4 expression was detected in differentiated cells at the lumen of seminiferous tubules (Figure 2C). Undifferentiated spermatogonia which are mainly localized along the base of the seminiferous epithelium appeared to be unaffected by *Mfn2* conditional deletion from germ cells at early spermatogenesis (Figures 2B and 2C). To confirm this result, we performed immunohistofluorescence (IHF) assays using an antibody against PLZF that marks undifferentiated spermatogonia. Indeed, PLZF+ cells were not evidently disturbed at P7, and their numbers were increased at P14 and P21 (Figures 2D, S2A, and S2B). Because MFN2 expression levels increased during spermatogonial differentiation (Figure 1E), we next examined whether MFN2 deficiency impairs the formation of differentiating spermatogonia. Flow cytometry analyses demonstrated an increased proportion of CD9+/KIT− undifferentiated spermatogonia in *Mfn2* knockout testes accompanied by substantially reduced KIT+ differentiating spermatogonia (Figure 2E). Notably, *Mfn1* conditional knockout mice (*Mfn1$^{f/f}$; Ddx4-Cre*, abbreviated as *Mfn1*

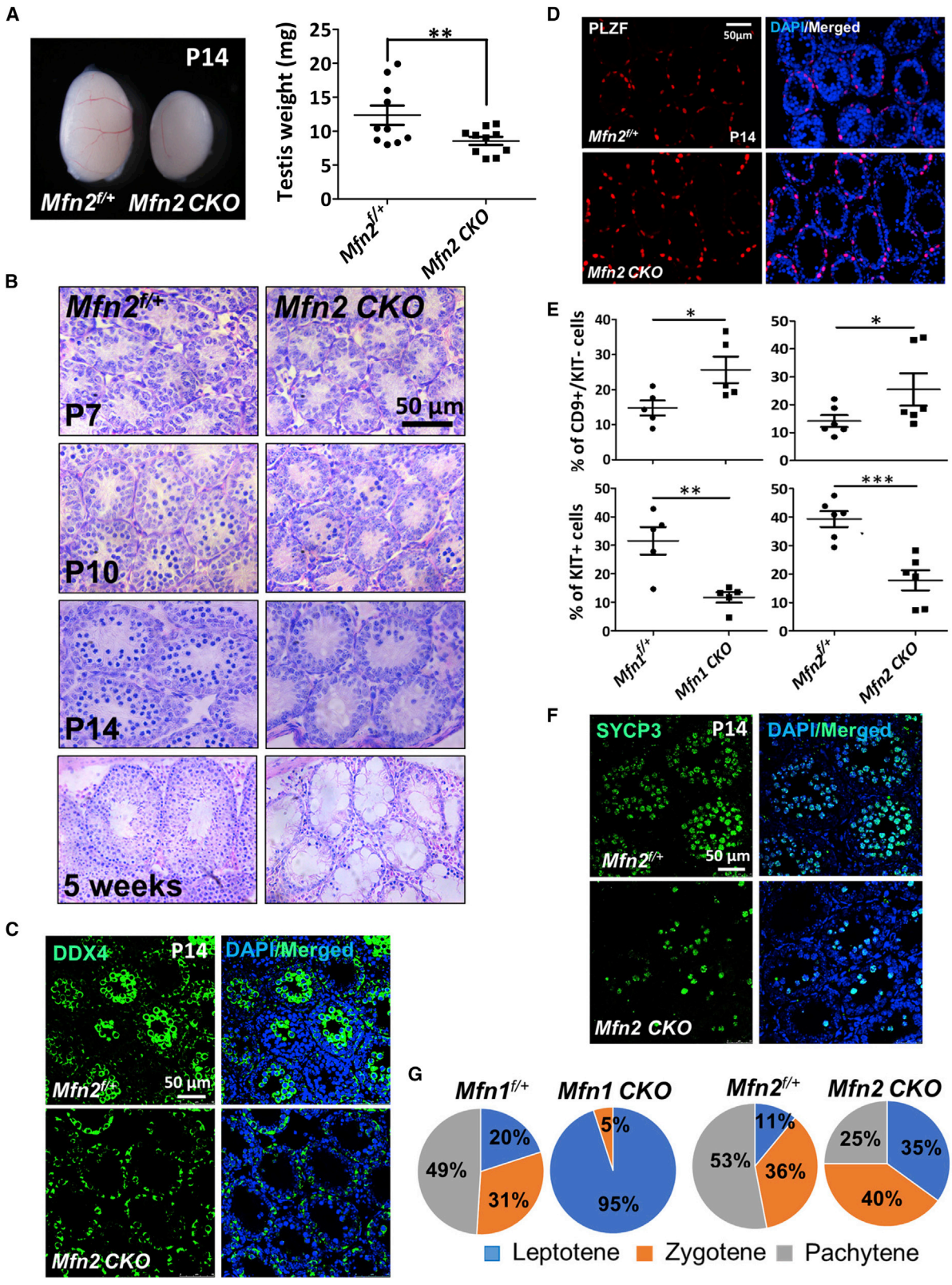

(legend on next page)

CKO in figures) displayed a similar spermatogonial differentiation block with MFN2 mutants (Figure 2E).

We further analyzed spermatocyte formation in *Mfn* null testes. IHF assays showed a significant reduction in SYCP3+ spermatocytes in *Mfn2$^{f/f}$; Ddx4-Cre* mice (Figure 2F), suggesting a meiotic arrest upon MFN2 deficiency, similar to a phenotype we previously observed in *Mfn1* conditional knockout mice (Zhang et al., 2016). To identify the exact stages of spermatocyte development that MFNs regulate, meiotic chromosome spreading assays were performed on both MFN1- and MFN2-deficient testes at P14. We found few zygotene spermatocytes in *Mfn1$^{f/f}$; Ddx4-Cre* mice, while meiotic arrest in *Mfn2$^{f/f}$; Ddx4-Cre* mice occurred at the pachytene stage (Figures 2G and S2C). These data reveal that MFN1 deficiency leads to a relatively earlier blockage of meiosis than that due to *Mfn2* conditional knockout in germ cells.

Mfn Conditional Knockout Causes Apoptosis Specifically in Differentiating Spermatogonia and Spermatocytes

To understand how spermatogonial differentiation and spermatocyte formation were blocked upon MFN2 deficiency, we first examined whether the proliferation of germ cells upon *Mfn2* deletion was affected by co-staining of PCNA (proliferating cell nuclear antigen) and the germ cell marker DDX4 at P7 and P14. No obvious change in PCNA expression was detected in DDX4+ cells of *Mfn2$^{f/f}$; Ddx4-Cre* mice compared with their control littermates (Figure 3A). By contrast, flow cytometry analyses using dual-staining of annexin V and propidium iodide (PI) demonstrated that PI+ apoptotic cells were significantly increased in the KIT+ population (Figure 3B). Annexin V+/PI− early apoptotic cells were slightly increased in CD9+/KIT− cells from *Mfn1$^{f/f}$; Ddx4-Cre* (Figure 3B), but cell death (PI+ cells) was negligible in CD9+/KIT− spermatogonia upon deletion of either *Mfn1* or *Mfn2* (data not shown). TUNEL assays further supported this result that apoptotic cells were mainly differentiated germ cells located in the lumen of testicular tubules (Figure S2D). Taken together, our data suggest that the impaired spermatogenesis upon MFN deficiency is likely due to increased apoptosis in differentiating spermatogonia and spermatocytes.

MFN Null Mutations Lead to Increased ROS Levels and DNA Oxidation in Differentiating Spermatogonia and Spermatocytes

The diverse mitochondrial functions regulated by mitochondrial dynamics vary by cell types. To determine the extent to which mitochondrial functions are impaired due to MFN deficiency during spermatogenesis, we first examined the mitochondrial membrane potential upon *Mfn* deletion in non-adherent germ cells collected from dissociated P12 testes using serial adhering procedures (Figure S1F). Indeed, we found the percentage of cells with lower mitochondrial potential was increased (Figures 4A and S3A), suggesting impaired mitochondrial functions upon conditional knockout of either *Mfn1* or *Mfn2*.

Because mitochondria serve as a powerhouse for ATP generation, we next assessed ATP generation in MFN mutants. To our surprise, ATP levels were not significantly altered in *Mfn*-deleted testes at P12 compared with their littermate controls (Figure 4B). Similar results were observed in GC1, an immortalized type B differentiating spermatogonial cell line (Hofmann et al., 1992). No significant alteration in ATP levels was observed upon downregulation of MFN1 or MFN2 expression by RNA interference (Figures S3B and S3C). However, upon the loss of function of either MFN, we observed increased ROS levels specifically in KIT+ cells (Figures 4C and S3D). By contrast, no significant changes in ROS production were detected in CD9+/KIT− undifferentiated spermatogonia (Figures 4C and S3D). Since high ROS levels cause DNA oxidation, we collected KIT+ germ cells from testes at P11 and stained them with an antibody against 8-oxoguanine, which is an indicator for DNA oxidation. Indeed, the 8-oxoguanine+ germ cells were significantly increased upon deletion of either *Mfn1* or *Mfn2* (Figure 4D). Notably, we did not observe significant changes in autophagy

Figure 2. Loss of Function of Either *Mfn* Blocks Spermatogonial Differentiation and Spermatocyte Formation

(A) Gross morphology of testes from mice at P14. Right panel: testis weights in P14 *Mfn2$^{f/+}$* and *Mfn2$^{f/f}$; Ddx4-Cre* mice were measured. Data represent mean ± 1 SEM. **p < 0.01; N = 10.

(B) Histological studies on *Mfn2$^{f/+}$* and *Mfn2$^{f/f}$; Ddx4-Cre* testes at various ages.

(C and D) IHF assays on testicle sections from *Mfn2$^{f/f}$; Ddx4-Cre* mice or *Mfn2$^{f/+}$* littermates at P14 with DDX4 (C) or PLZF (D) antibodies.

(E) Percentage of CD9+/KIT− undifferentiated spermatogonia and KIT+ differentiated spermatogonia in P12 testes were determined by flow cytometry. Data are presented as mean ± 1 SEM. *p < 0.05, **p < 0.01, ***p < 0.001; n ≥ 5.

(F) IHF on *Mfn2$^{f/+}$* and *Mfn2$^{f/f}$; Ddx4-Cre* testes from P14 mice with an antibody against SYCP3.

(G) Meiosis chromosome/DNA spreading assay was performed with antibodies against SYCP3 and γ-H2A.X on testes from P14 mice. The percentage of primary spermatocytes at different stages of prophase I was calculated according to the chromatin structure and staining of γ-H2A.X. *CKO*: conditional deletion of *Mfn1* or *Mfn2* in germ cells by *Ddx4-Cre*.

See also Figure S1.

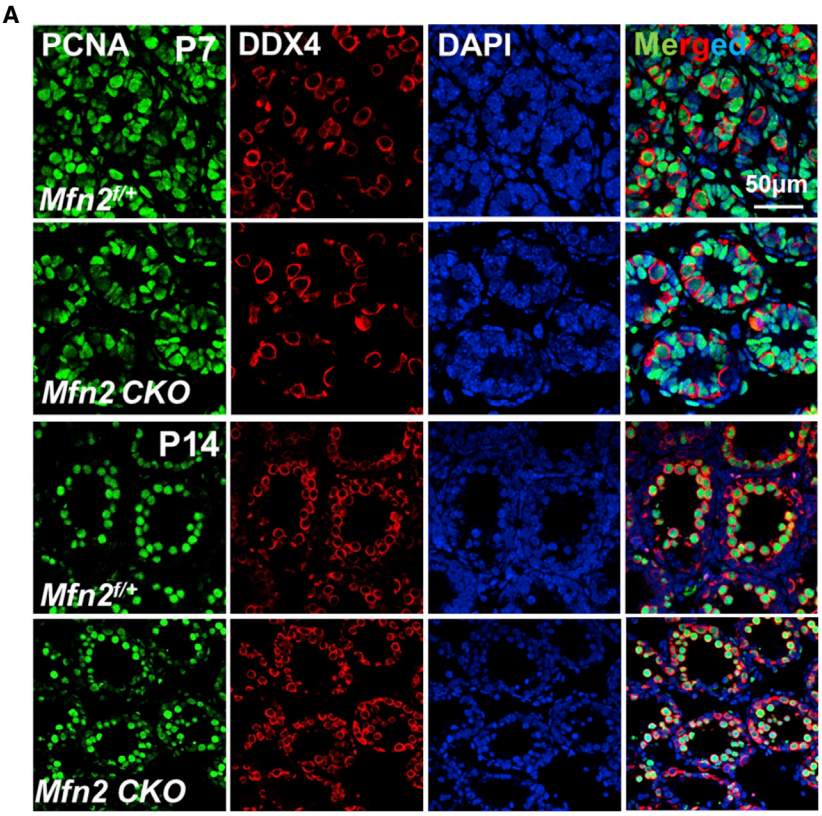

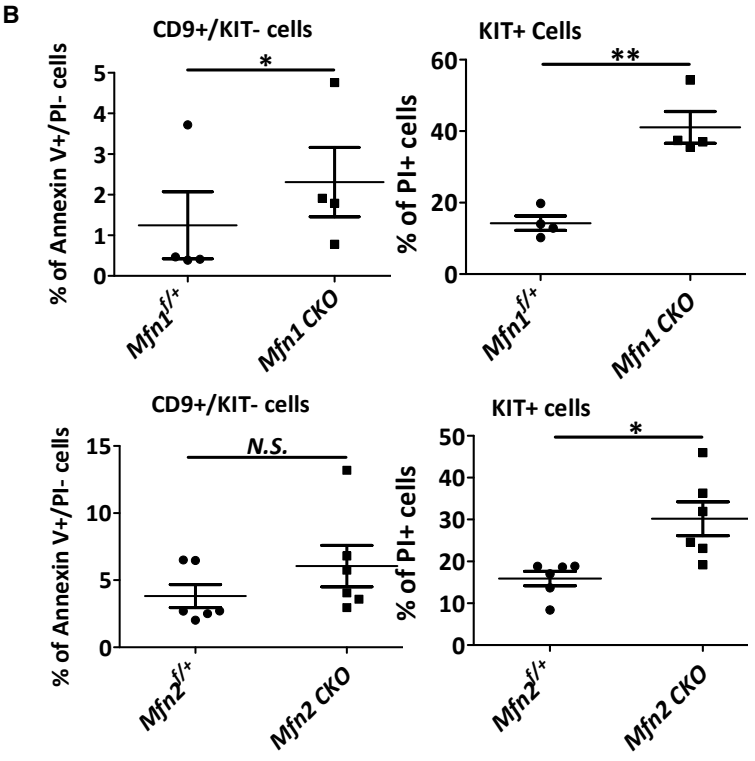

Figure 3. MFN Deficiency Leads to Apoptosis in Differentiating Spermatogonia and Spermatocytes

(A) IHF with PCNA and DDX4 co-staining on *Mfn2*$^{f/+}$ and *Mfn2*$^{f/f}$; *Ddx4-Cre* testes at P7 and P14.

(B) Percentage of apoptotic cells was analyzed by flow cytometry with FITC-Annexin V and PI co-staining on CD9+/KIT− undifferentiated spermatogonia and KIT+ cells collected from testes of P12 mice. Data represent mean ± 1 SEM from at least four littermate pairs. *p < 0.05, **p < 0.01; N.S., no statistical significance. See also Figure S2.

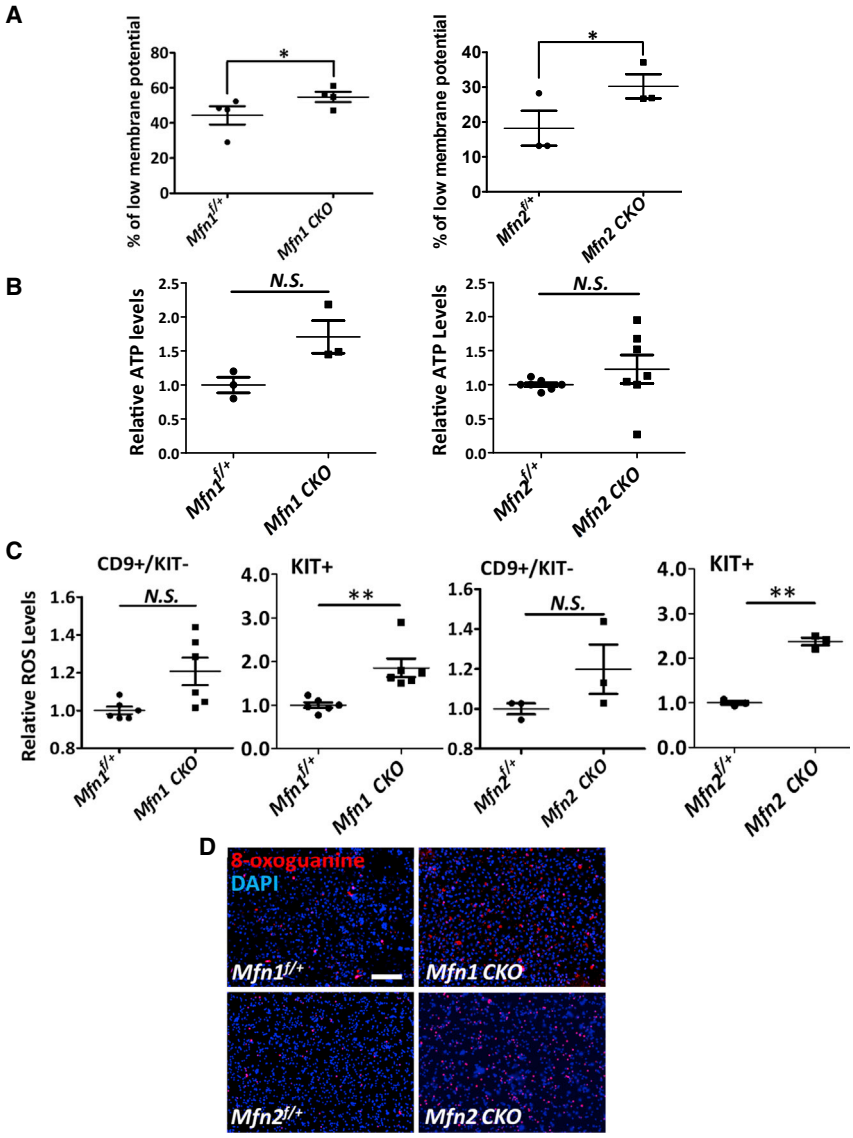

Figure 4. *Mfn* Deletion Causes Mitochondrial Dysfunction and Elevated DNA Oxidation

(A) Percentage of cells with low mitochondrial membrane potential was measured with flow cytometry in non-adherent germ cells collected from testes of P12 mice.

(B) ATP levels were measured on dissociated cells from P12 testes, calculated in comparison with their littermate controls.

(C) ROS levels were analyzed by flow cytometry in CD9+/KIT− undifferentiated spermatogonia and KIT+ differentiating germ cells from testes of P12 mice.

(D) Immunofluorescence (IF) with an antibody against 8-oxoguanine on sorted KIT+ germ cells from mice at P11. Scale bar, 2 mm.

(A–C) Data are presented as mean ± 1 SEM. N ≥ 3. *p < 0.05, **p < 0.01; N.S., no statistical significance. See also Figure S3.

(Figure S4A), piRNA levels (Figure S4B), and expression levels of transposable elements (Figure S4C) upon *Mfn2* conditional knockout. Therefore, we conclude that the increased cell death in MFN-deficient germ cells is not directly caused by altered energy production, autophagy, or piRNA biogenesis, but rather due to DNA damage from increased oxidation.

Loss of Function of MFN1 and MFN2 Causes Distinct Defects in Mitochondrial Architecture at Different Stages of Spermatogenesis

As described above, mitochondrial functions were disturbed by either MFN1 or MFN2 deficiency. To directly visualize the underlying mitochondrial defects due to *Mfn* deletion, we closely examined alterations in mitochondrial morphology and architecture of germ cells by transmission electron microscopy (TEM) at various time points during early spermatogenesis. We found normal mitochondrial morphology at P0 in *Mfn2* knockout pro-spermatogonia (Figure 5A). At P5, mitochondrial morphology started to vary, with a small fraction appeared to be rounded up and contained less cristae (Figure 5B, right panel) upon the loss of function of MFN2. Between P8 and P11, the majority of mitochondria in *Mfn2$^{f/f}$; Ddx4-Cre* germ cells became swollen and enlarged (Figures 5C and 5D) compared with their littermate controls. In addition, differentiated germ cells that were located toward the lumen of testicular tubules displayed more severe abnormalities than undifferentiated spermatogonia (Figure 5C, right two panels).

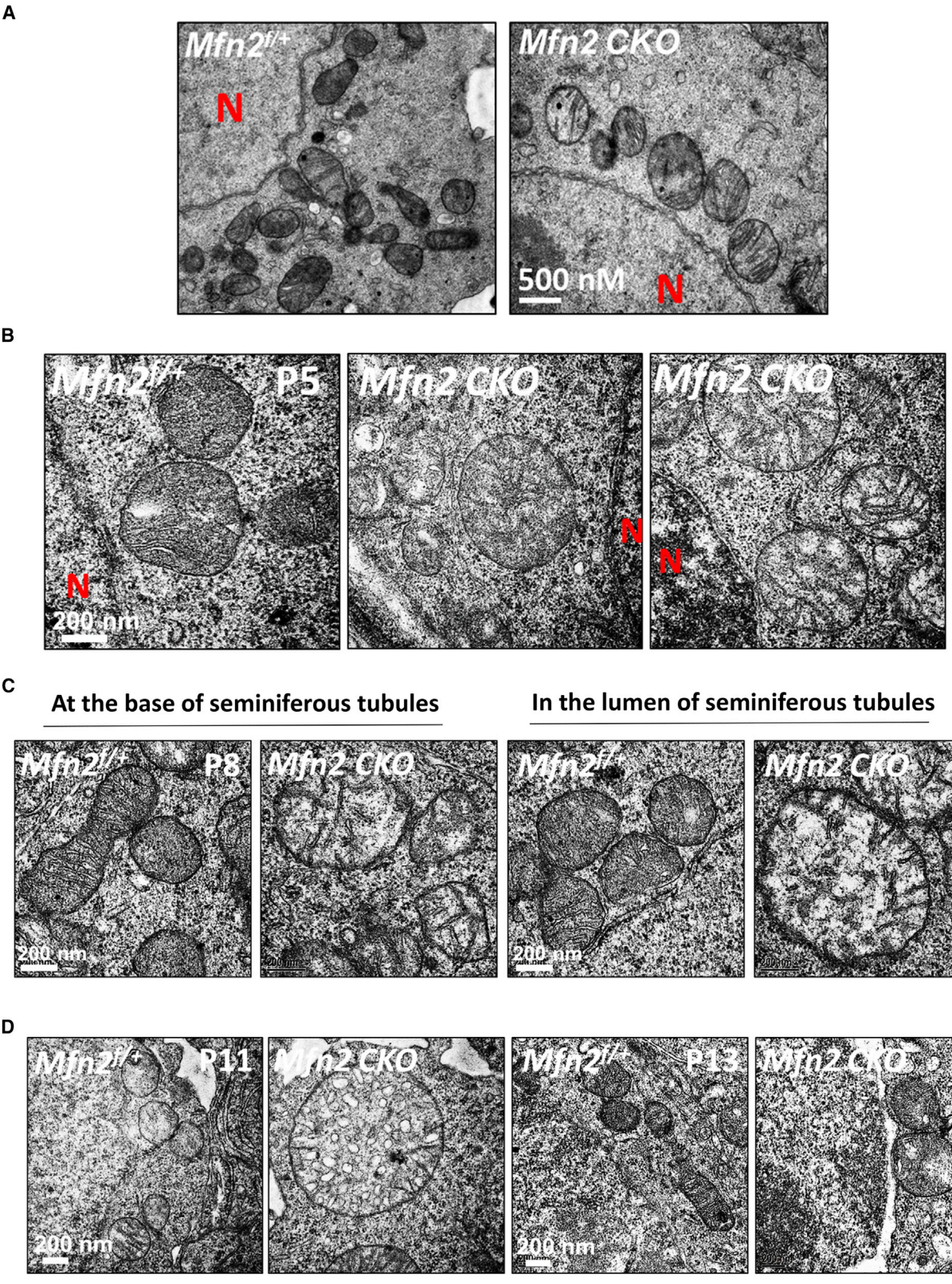

(legend on next page)

Intriguingly, mitochondria in *Mfn2*-deleted germ cells returned to relatively normal size around P13, but few tubular mitochondria were detected (Figure 5D, right two panels).

The exact stages that abnormalities of mitochondrial features occurred in *Mfn2* knockout appeared to be different from the ones we had previously detected in MFN1 mutants (Zhang et al., 2016). *Mfn1* conditional deletion in DDX4+ germ cells caused severely swollen and significantly enlarged mitochondria in neonatal (P0) prospermatogonia compared with their littermate controls (Zhang et al., 2016). To further reveal the differential impacts of *Mfn1 and Mfn2* knockout on mitochondrial features, we examined mitochondrial morphology and architecture by TEM in *Mfn1*-deleted germ cells at various time points of early spermatogenesis. Interestingly, mitochondria in *Mfn1* knockout germ cells also displayed dynamical alterations during spermatogenesis. They became round mitochondria with normal size at P5 and were then substantially smaller at P8 compared with their littermate controls (Figure S4D). In summary, our results demonstrate that either *Mfn1* or *Mfn2* deletion causes mitochondrial defects that, however, vary at different time points during early spermatogenesis.

Both Mitochondrial and ER Dysregulation Contribute to Male Infertility Caused by MFN2 Deficiency

Based on our results above, MFN1 appears to play a dominant role in regulating mitochondrial features at early time points of spermatogenesis (i.e., before P5). Compared with *Mfn1* knockout, *Mfn2* deletion only led to relative mild defects in mitochondrial morphology and architecture at later stages during spermatogenesis (P8–P11). Nevertheless, MFN2 deficiency blocked spermatogonial differentiation and eventually led to male infertility, similar to what we observed in MFN1 null mutants. This indicates the existence of other mechanisms that underlie impaired germ cell development due to MFN2 deficiency. It was reported that, in fibroblasts and certain types of neurons, MFN2 affected mitochondrial functions indirectly by regulating mitochondrion-ER interaction and ER homeostasis (Chen et al., 2003, 2007; de Brito and Scorrano, 2008; Dietrich et al., 2013; Schneeberger et al., 2013). We observed upregulated ER activities and increased expression of MFNs during spermatogonial differentiation (Figure 1). Therefore, we examined whether MFN2 regulates ER functions in germ cell development.

Because ER is the major Ca^{2+} reservoir, and ER disturbance leads to abnormal Ca^{2+} homeostasis, we first analyzed cellular Ca^{2+} levels in germ cells from *Mfn2*$^{f/+}$ and *Mfn2*$^{f/f}$*; Ddx4-Cre* mice by flow cytometry with Fluo4-AM, a fluorescent Ca^{2+} indicator. We also examined Ca^{2+} levels in *Mfn1* conditional knockout mice for comparison purposes. No significant changes were detected in *Mfn1*$^{f/f}$*; Ddx4-Cre* germ cells, while *Mfn2* deletion led to a substantial increase in cellular Ca^{2+} levels compared with their control littermates (Figures 6A and S5A). The increase in Ca^{2+} levels upon *Mfn2* deletion started in CD9+/KIT− undifferentiated spermatogonia and became more dramatic in KIT+ cells (Figure 6B). Similar phenomena were observed in GC1 type B spermatogonial cells (Figure S5B). No significant alteration of cellular Ca^{2+} levels was observed upon downregulation of MFN1 expression by RNA interference, but substantially increased Ca^{2+} levels were detected upon MFN2 knockdown (Figure S5B). To assess whether increased cellular Ca^{2+} levels affects mitochondrial Ca^{2+} storage, we further examined mitochondrial Ca^{2+} levels in *Mfn1*- or *Mfn2*-deleted germ cells. We found that mitochondrial Ca^{2+} levels dramatically increased upon *Mfn2* knockout, as displayed by increased co-staining of Fluo3-AM, a fluorescent Ca^{2+} indicator similar to Fluo 4-AM, and a MitoTracker to specifically label mitochondria (Figure 6C). By contrast, no significant alteration in mitochondrial Ca^{2+} level was found in *Mfn1*$^{f/f}$*; Ddx4-Cre* germ cells compared with their littermate controls (Figure 6C). Notably, we found an increased percentage of fragmented ER in *Mfn2*-deleted germ cells at P5 by TEM (Figures 6D and S5C). This finding was further supported by multiplexed 3D super-resolution confocal microscopy with Tomm20 (to label mitochondria) and calreticulin (to mark ER) co-staining, which showed swollen mitochondria and fragmented ER in *Mfn2*-deleted germ cells (Figure S5D). Taken together, these data reveal a disturbed cellular and mitochondrial Ca^{2+} homeostasis upon *Mfn2* but not *Mfn1* deletion, probably due to Ca^{2+} released from ER caused by its fragmentation.

As disturbed ER homeostasis usually leads to upregulation of chaperone genes to restore ER functions, we next assessed the expression levels of ER stress markers and ER chaperons by real-time RT-PCR and western blotting. Indeed, expression levels of several ER stress markers

Figure 5. Ultrastructural Changes of Mitochondria upon *Mfn2* Deletion

Mitochondrial architecture was examined by TEM on testicular sections from *Mfn2* conditional knockout testes and littermate controls during spermatogenesis at P0 (A), P5 (B), P8 (C), and P11 and P13 (D). At P5 (B), a small fraction of round mitochondria containing less cristae are shown in the right panel. At P8 (C), the left two panels show mitochondrial morphology in undifferentiated spermatogonia at the basal membrane of the seminiferous tubule. Mitochondria from differentiated cells located toward the lumen of tubules are displayed in the two right panels. N, nucleus. See also Figure S4.

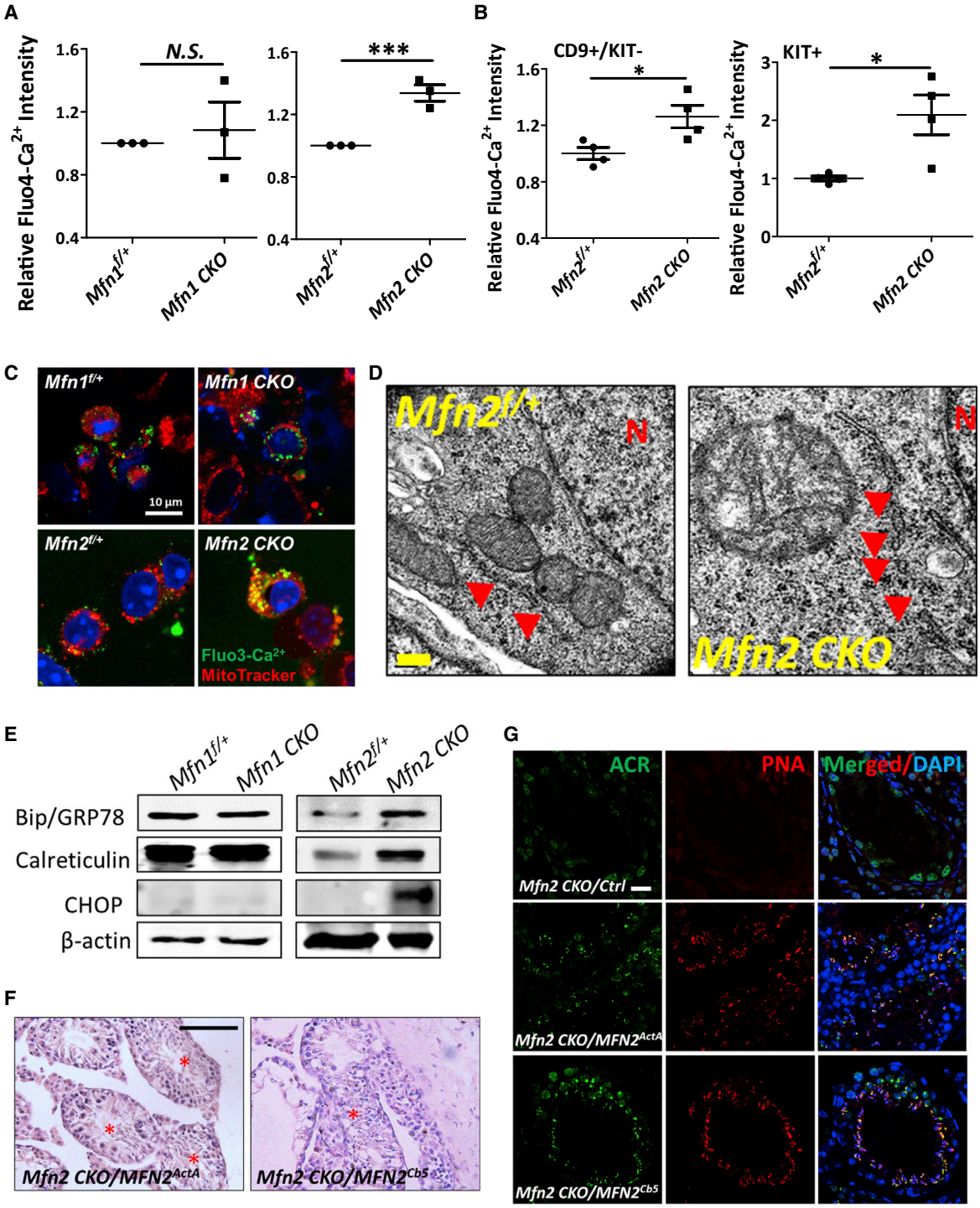

Figure 6. MFN2 Regulates Both Mitochondrial and ER Functions in Germ Cells

(A and B) Fluo4-AM fluorescent intensity was measured by flow cytometry on non-adherent germ cells (A), as well as sorted CD9+/KIT− undifferentiated and KIT+ differentiating spermatogonia (B) from testes of P11 mice. Data are presented as mean ± 1 SEM from three biological replicates. ***$p < 0.001$; N.S., no statistical significance.

(C) IF on non-adherent germ cells from P11 testes with green Fluo3-AM probe (to indicate Ca^{2+} level) and a red mitochondrial tracker.

(D) Mitochondrial and ER architectures were examined by TEM on testicular sections from *Mfn2*$^{f/+}$ and *Mfn2*$^{f/f}$*; Ddx4-Cre* testes of P5 mice. Red arrows indicate ER. N, nucleus.

(legend continued on next page)

(calreticulin and CHOP) and ER chaperon GPR78 were significantly increased in *Mfn2*$^{f/f}$*; Ddx4-Cre* testes but not in *Mfn1*-deleted mutants (Figure 6E). Similar results were observed in *Mfn2*$^{f/f}$*; Ddx4-Cre* non-adherent germ cells (Figure S5E, left panel), sorted spermatogonia (Figure S5E, right panel) from *Mfn2*$^{f/f}$*; Ddx4-Cre* testes, and GC1 cells upon MFN downregulation by RNA interference (Figure S5F), thereby suggesting that ER homeostasis was disturbed upon *Mfn2* deletion.

Both mitochondrial and ER functions are impaired by MFN2 deficiency, it is therefore unclear whether the male infertility upon *Mfn2* deletion is due to dysfunctional mitofusion, ER stress, or both. Recent data suggest a partial localization of MFN2 at ER and mitochondrion-ER contacts (de Brito and Scorrano, 2008; Schneeberger et al., 2013). To answer this question, lentiviral vectors were constructed to express MFN2 that were specifically tagged either to the surfaces of mitochondria (MFN2^{ActA}) or to ER (MFN2^{Cb5}) by localization signaling peptides (de Brito and Scorrano, 2008; Schneeberger et al., 2013). We then introduced these viruses to *Mfn2*$^{f/f}$*; Ddx4-Cre* mice through testicular seminiferous tubule injection (Gou et al., 2017; Ikawa et al., 2002; Li et al., 2013) and examined the germ cell development around days 30–40 after viral transduction. The MFN2 expression from these viral vectors was confirmed in both immortalized *Mfn2*$^{-/-}$ mouse embryonic fibroblasts (Chen et al., 2003) with the same viral infection (Figure S6A) and testis after viral injection (Figure S6B). Strikingly, we found fully developed haploid spermatids in seminiferous tubules of *Mfn2*$^{f/f}$*; Ddx4-Cre* testes upon the introduction of MFN2 proteins, either localized at mitochondrial membrane or at ER (Figures 6F and S6C). We further performed IHF with an antibody against acrosin (ACR) or with rhodamine-labeled peanut agglutinin (PNA) to detect acrosome that only exists in haploid spermatids and spermatozoa. Consistent with our histological observations, ACR+ and PNA+ spermatids were clearly observed in *Mfn2*$^{f/f}$*; Ddx4-Cre* testes rescued with either mitochondrion- or ER-localized MFN2 (Figures 6G and S6D). Taken together, our data reveal that MFN2 contributes to male germ cell development by regulating both mitochondrial and ER functions.

Because both MFN1 and MFN2 promote mitochondrial fusion, we further tested whether MFN1 compensates the defects of germ cell development caused by *Mfn2* deletion, or vice versa. We introduced the viruses expressing MFN1 into both *Mfn1*$^{f/f}$*; Ddx4-Cre* and *Mfn2*$^{f/f}$*; Ddx4-Cre* testes and examined their germ cell development. ACR+ and PNA+ spermatids were detected in *Mfn1*$^{f/f}$*; Ddx4-Cre* testes but not in *Mfn2*$^{f/f}$*; Ddx4-Cre* mice injected with *Mfn1*-expressing virus (Figure S6D). Similarly, *Mfn2* transgene did not rescue blocked germ cell development from *Mfn1*$^{f/f}$*; Ddx4-Cre* mice (Figure S6D). Therefore, we conclude that MFN1 and MFN2 play non-redundant roles in regulating male germ cell development.

DISCUSSION

Although the machinery for mitochondrial fusion has been extensively investigated in somatic cells, its role in germline stem cell differentiation under developmental settings remains elusive. In this study, along with increased ROS generation during postnatal germ cell development, we detected upregulated expression of both MFN1 and MFN2, two GTPases critical for mitochondrial fusion. We found that loss of function of either MFN blocked spermatogonia differentiation and spermatocyte formation, which in turn led to male infertility. These phenotypes in MFN mutants were accompanied by altered mitochondrial morphology, architecture, and function, supporting a critical requirement of MFN-mediated mitochondrial activities during early spermatogenesis.

The cellular reliance on mitochondrial functions varies by cell type and developmental stage. Between stem cells or progenitors and the cells into which they differentiate, mitochondria have stage-specific functions, as shown by studies on pluripotent stem cells, neural stem cells (NSCs), hematopoietic stem cells, and muscle stem cells (Bracha et al., 2010; Figueroa et al., 2010; Khacho et al., 2016; Mandal et al., 2011; Shyh-Chang et al., 2013; Son et al., 2015; Wanet et al., 2015; Zhou et al., 2012). These changes in mitochondrial functions and activities in turn impact the intrinsic programming of specification of stem cell fate. For example, mitochondrial features of NSCs are remarkably different from their committed progenitors, and disrupting mitochondrial fusion specifically impairs NSC self-renewal via ROS-NRF2-mediated retrograde (mitochondria to nucleus) signaling

(E) Expression levels of chaperon proteins were examined by western blots on testes from P12 mice.
(F) Histological studies of testicle sections from *Mfn2*$^{f/f}$*; Ddx4-Cre* mice at day 30 after viral introduction of MFN2 tagged with mitochondrion (*MFN2*^{ActA}) or ER (*MFN2*^{Cb5}) localization signals. Red stars indicate the seminiferous tubules containing haploid spermatids. Scale bar, 50 μm.
(G) IHF analyses with an antibody against acrosin (ACR), counterstained with peanut agglutinin (PNA) and DAPI on *Mfn2*$^{f/f}$*; Ddx4-Cre* testis sections at day 30 after viral introduction with ActA- or Cb5-tagged MFN2 through seminiferous tubules. Ctrl, control viruses produced with the empty vector. Scale bar, 20 μm.
(F and G) Three to four mice per group were used for viral injection. See also Figures S5 and S6.

(Khacho et al., 2016). By contrast, inhibition of mitochondrial fusion during reprogramming upregulates the formation of induced pluripotent stem cells (Son et al., 2015). In our study, we found upregulated mitochondrial functions in KIT+ differentiation spermatogonia, as indicated by increased ROS levels and MFN expression. Although *Mfn* deletion caused defects in mitochondrial morphology and architecture in spermatogonia, the numbers of CD9+/KIT− or PLZF+ undifferentiated spermatogonia increased upon *Mfn* knockout compared with their littermate controls. Conversely, the formation of KIT+ differentiating spermatogonia and primary spermatocytes was specifically blocked. Our data, therefore, suggest that spermatogonial differentiation and meiosis are particularly sensitive to mitochondrial defects, likely due to a high basal dependence on mitochondrial functions in differentiated germ cells. The differential sensitivity to disrupted mitochondrial dynamics across hierarchical lineages thus reflects the importance of mitochondrial regulation in germ cell development.

Our data further reveal that the blockage of spermatogonial differentiation and meiosis upon *Mfn* deletions is likely due to increased apoptosis in differentiated cell populations. Although clustered mitochondria are the essential components of IMC, a unique subcellular structure for piRNA biogenesis, no alteration was observed in the expression of transposable elements and piRNAs from *Mfn*-deleted germ cells. Furthermore, despite the classic role of mitochondria as a powerhouse, ATP production was not decreased either at the time points when significant apoptosis occurred in *Mfn* knockout. By contrast, ROS level was significantly upregulated in KIT+ cells, which in turn led to increased DNA damage due to oxidation, as supported by increased 8-oxoguanine formation—an indicator for DNA oxidation in *Mfn*-deficient germ cells. In addition, *Mfn2* deletion also led to increased cellular and mitochondrial Ca^{2+} levels, which disturbs cellular Ca^{2+} signaling and sensitizes cells to apoptosis (de Brito and Scorrano, 2008; Filadi et al., 2015). Therefore, we conclude that high DNA oxidation and pathologically increased Ca^{2+} levels are at least partially responsible for germ cell apoptosis upon MFN2 deficiency. This conclusion does not contradict to our finding that ROS and Ca^{2+} levels increase during germ cell development. One may speculate that physiologically controlled ROS and Ca^{2+} elevation from upregulated mitochondrial and ER activities are required for spermatogonial differentiation; however, abnormal ROS or Ca^{2+} elevation beyond pathological thresholds will cause excessive DNA oxidation/damage and dysfunctional Ca^{2+} signaling, and in turn lead to cell death. Our findings thus highlight the levels of mitochondrial and ER activities need to be precisely controlled by MFNs to maintain proper germ cell development.

In somatic cells, such as fibroblasts, deleting either *Mfn1* or *Mfn2* directly leads to mitochondria fragmentation (Chen et al., 2003). Interestingly, in *Mfn* knockout germ cells we were able to observe a dynamic alteration of mitochondrial morphology and architecture during spermatogenesis. Before fragmentation, mitochondria were first enlarged and swollen with vesiculation of the mitochondrial inner membrane. It is possible that, at early stages of MFN deficiency, impaired mitofusion leads to a feedback downregulation in mitochondrial fission which causes enlarged mitochondria. However, as MFN deficiency continues, reduced mitochondrial fission is no longer able to compensate the severely compromised mitofusion, which eventually leads to small and fragmented mitochondria in *Mfn*-deleted germ cells.

MFN1 and MFN2 share more than 80% similarity in their protein sequences, and they are expressed in germ cells at comparable levels. However, our data show that deletion of either *Mfn* leads to male infertility, and they likely play distinctive and non-redundant roles in spermatogenesis. MFN1 re-introduction into testes restored spermatogenesis in *Mfn1$^{f/f}$; Ddx4-Cre* mice but not in *Mfn2* conditional knockout, and vice versa. Compared with MFN2, MFN1 deficiency affected mitofusion at earlier stages of spermatogenesis. In addition, MFN2 regulated mitochondrial functions directly through mitofusion and possibly indirectly via ER homeostasis, as supported by altered mitochondrial and ER architectures in MFN2-deficient germ cells. Introduction of either mitochondrion- or ER-localized MFN2 rescued the defects in spermatogenesis due to *Mfn2* deletion. Previous studies suggest that MFN2 regulates mitochondrion-ER contacts in embryonic fibroblasts and in certain neurons (de Brito and Scorrano, 2008; Schneeberger et al., 2013). However, in germ cells, we did not observe consistent alterations in mitochondrion-ER juxtaposition upon *Mfn2* knockout. This may be explained by cell-type-specific regulatory mechanisms of MFN2 on mitochondria and ER activities. For example, MFN2 deficiency in POMC neurons causes diet-induced obesity due to defects in mitochondrion-ER juxtaposition (Schneeberger et al., 2013), whereas in agouti-related peptide neurons or Purkinje cells, MFN2 mutations mainly lead to dysfunctional mitochondrial fusion (Chen et al., 2007; Dietrich et al., 2013). Our data not only delineate crucial and unique contributions of MFN2 to both mitochondrial and ER components during germ cell development, but also indicate an essential coordination between MFN1 and MFN2 during spermatogonial differentiation.

Infertility affects approximately 48.5 million couples worldwide, with half due to male factors (Agarwal et al., 2015). This public health problem is further compounded by an increasing prevalence of metabolic disorders, particularly obesity and diabetes, which are linked to male

infertility (Du Plessis et al., 2010). Notably, MFN2 mutations have been identified from patients with metabolic alterations (Bach et al., 2003; Rovira-Llopis et al., 2017). Our data demonstrate that deletion of either *Mfn1* or *Mfn2* impairs mitochondrial functions and destroys male fertility, providing an important connection between mitochondrial metabolic disorders and impaired spermatogenesis. Further research into this connection may lead to an important gateway to treat male infertility.

EXPERIMENTAL PROCEDURES

Generation of Conditional Mfn2 Knockout Mice

Sperm harboring the floxed *Mfn2* allele were obtained from Mutant Mouse Regional Resource Center (MMRRC at UC Davis, USA, resource identifier no. MMRRC_029902-UCD). *Mfn2*$^{f/+}$ mice were derived by intracytoplasmic injection of sperm into oocytes and maintained by crossing with C57BL/6 mice. *Ddx4-Cre* mice (Model Animal Research Center at Nanjing University, China) were used to obtain targeted *Mfn2* deletion in germ cells. *Mfn2*$^{f/f}$*; Ddx4-Cre* mice were generated by *Mfn2*$^{f/f}$ female mice crossing with *Mfn2*$^{f/+}$*; Ddx4-Cre* males. Conditional *Mfn1* knockout mice were generated in the same way by intracytoplasmic injection of sperm (MMRRC_029901-UCD) as described previously (Zhang et al., 2016). Animal use protocols for this study were approved by the Institutional Animal Care and Use Committee of East China Normal University (project no. AR201305006) and all experiments were carried out in accordance with approved protocols.

Seminiferous Tubule Injection with Lentivirus

Mfn2 cDNAs tagged with sequences encoding a mitochondrial (ActA) or an ER (Cb5) localization signal (Chen et al., 2003; Schneeberger et al., 2013) (kind gifts from Dr. Luca Scorrano from the Venetian Institute of Molecular Medicine, Italy) were amplified by PCR and cloned into *pll3.7-EF1α-Mfn2-IRES-Hygro*, a lentiviral vector. All constructs were verified by DNA sequencing. Lentiviral vectors expressing *Mfn1* or *Mfn2* full-length cDNAs were reported previously (Zhang et al., 2016). Lentiviral injection was performed according to published protocols (Gou et al., 2017; Ikawa et al., 2002; Li et al., 2013). In brief, *Mfn1*$^{f/f}$*; Ddx4-Cre* or *Mfn2*$^{f/f}$*; Ddx4-Cre* mice at 3 weeks were injected with 5 μL of lentivirus through the testicular seminiferous tubule and examined by histology and IHF at days 30–40 after injection.

Histology and IHF Assays

For histology study, mouse testes were fixed in Bouin's fixative at 4°C overnight for staining with hematoxylin and eosin as described previously (Wang et al., 2017). For IHF, testes were fixed with 4% paraformaldehyde in PBS at 4°C overnight and embedded in paraffin. The 4-μm-thick testicular sections were incubated with primary antibodies and washed three times with PBS containing 0.5% Tween 20. Nuclei were stained in 0.5 μg/mL DAPI after blotting with FITC- or TRITC-conjugated second antibodies. Slides were imaged under a fluorescent microscope (Leica, DM400BLED368424) or a Lecia TCS/SP5 confocal microscope and processed with Image-Pro Plus. Antibodies and fluorescent probes used in this study: PLZF (Santa Cruz Biotechnology, SC-28319), DDX4 (Abcam, ab13840), SYCP3 (Abcam, ab15093), PCNA (Abcam, ab29), Acrosin/ACR (Atlas Antibodies, HPA048687), rhodamine-labeled PNA (Vector Laboratories, RL-1072), Alexa Fluor 488- or TRITC-conjugated anti-mouse, or anti-rabbit secondary antibodies (Jackson ImmunoResearch).

TEM

TEM was performed as described previously (Zhang et al., 2016). In brief, mouse testes were fixed with 2.5% TEM-grade glutaraldehyde in 0.1 M PBS (pH 7.4) overnight and incubated in 1% osmium tetroxide for 2 h at 4°C in the dark. After dehydration in ethanol with increasing concentration from 30% to 90%, samples were treated in 45% ethanol and acetone at 4°C for 15 min, and then in 100% acetone three times before further embedding, slide processing, and staining. Sample grids were examined using a Hitachi H7500 transmission electron microscope.

Flow Cytometry

Testes were digested into single cells and cell surface antigens were stained with fluorochrome-conjugated CD90 or CD9 and KIT antibodies for 40 min on ice and washed with PBS before analyses. For ROS detection, cells were stained with 5 μM H_2DCFDA (Thermo Fisher Scientific, D399) in PBS containing 1% BSA at 37°C for 40 min in the dark followed by washing with PBS twice. For analyses of mitochondrial membrane potential, cells were stained with JC-1 dye (Beyotime Biotechnology, C2006) at 37°C for 40 min following the manufacturer's instructions. For the apoptosis test, cells were stained with FITC-Annexin V and PI using an FITC-Annexin V Apoptosis Detection Kit (BD Biosciences, 556420). To determine Ca^{2+} levels, cells were stained with 2 μM Fluo-4 AM (Beyotime Biotechnology, S1060) in PBS containing 1% BSA at 37°C for about 40 min. Flow cytometry analyses and sorting were performed on a Fortessa analyzer and an Aria II cell sorter (BD Biosciences), respectively. Antibodies below were used with 2 μg/mL per 1–2 million cells as a final working concentration: APC-CD9 (17-0091-82, eBioscience, USA); APC-CD90.2 (105311) and FITC-KIT (105806) from BioLegend, USA, and PE-KIT (553355, BD Biosciences, USA).

RT-PCR, PCR, and Real-Time PCR

Total RNA from cultured cells was extracted by using TRIzol (Thermo Fisher Scientific) and reverse-transcribed by using a cDNA Synthesis Kit (Takara Biotechnology). PCR and real-time PCR were performed on a Bio-Rad thermal cycler (Bio-Rad) or on a Stratagene Mx3000P (Stratagene, CA, USA). Three or more technical replicates were conducted for each independent experiment. Sequences of primers used in this study are provided in Table S1.

Meiotic Chromosome Spreading Assays, Immunofluorescence Assays, Measurement of ATP Levels, and Western Blotting

All assays were performed following standard procedures, with details of antibody/probe/dye information in Supplemental Experimental Procedures.

Statistical Analysis

Data are presented as mean ± SEM. All experiments were performed independently three times or more unless otherwise stated. Statistical significance of between-group differences was analyzed with unpaired Student's t test using the Prism Graphic software.

SUPPLEMENTAL INFORMATION

Supplemental Information can be found online at https://doi.org/10.1016/j.stemcr.2020.03.024.

AUTHORS CONTRIBUTIONS

W.C., Y.S., Q.S., J.Z., M.J., C.C., X.H., C.W., P.W., and Z.Z. performed the research. W.C., X.C., and Y.W. analyzed the data. Y.W. designed the experiments and wrote the article.

ACKNOWLEDGMENTS

We thank Dr. Luca Scorrano from Venetian Institute of Molecular Medicine for providing ActA- and Cb5-tagged MFN2 expression plasmids, and Dr. Mofang Liu from Chinese Academy of Sciences for help in piRNA detection. This work was supported by grants from the Ministry of Science and Technology of the People's Republic of China (2016YFA0100300), the National Natural Science Foundation of China (91854123 and 31771655). C.C., Z.Z., and Y.W. were supported by the NIFA through the AgbioResearch Hatch Fund from Michigan State University.

Received: September 11, 2019
Revised: March 27, 2020
Accepted: March 27, 2020
Published: April 23, 2020

REFERENCES

Agarwal, A., Mulgund, A., Hamada, A., and Chyatte, M.R. (2015). A unique view on male infertility around the globe. Reprod. Biol. Endocrinol. *13*, 37.

Bach, D., Pich, S., Soriano, F.X., Vega, N., Baumgartner, B., Oriola, J., Daugaard, J.R., Lloberas, J., Camps, M., Zierath, J.R., et al. (2003). Mitofusin-2 determines mitochondrial network architecture and mitochondrial metabolism. A novel regulatory mechanism altered in obesity. J. Biol. Chem. *278*, 17190–17197.

Bracha, A.L., Ramanathan, A., Huang, S., Ingber, D.E., and Schreiber, S.L. (2010). Carbon metabolism-mediated myogenic differentiation. Nat. Chem. Biol. *6*, 202–204.

Bukau, B., Weissman, J., and Horwich, A. (2006). Molecular chaperones and protein quality control. Cell *125*, 443–451.

Chan, D.C. (2006). Dissecting mitochondrial fusion. Dev. Cell *11*, 592–594.

Chen, H., Detmer, S.A., Ewald, A.J., Griffin, E.E., Fraser, S.E., and Chan, D.C. (2003). Mitofusins Mfn1 and Mfn2 coordinately regulate mitochondrial fusion and are essential for embryonic development. J. Cell Biol. *160*, 189–200.

Chen, H., McCaffery, J.M., and Chan, D.C. (2007). Mitochondrial fusion protects against neurodegeneration in the cerebellum. Cell *130*, 548–562.

Chuma, S., Hosokawa, M., Tanaka, T., and Nakatsuji, N. (2009). Ultrastructural characterization of spermatogenesis and its evolutionary conservation in the germline: germinal granules in mammals. Mol. Cell. Endocrinol. *306*, 17–23.

de Brito, O.M., and Scorrano, L. (2008). Mitofusin 2 tethers endoplasmic reticulum to mitochondria. Nature *456*, 605–610.

De Martino, C., Floridi, A., Marcante, M.L., Malorni, W., Scorza Barcellona, P., Bellocci, M., and Silvestrini, B. (1979). Morphological, histochemical and biochemical studies on germ cell mitochondria of normal rats. Cell Tissue Res. *196*, 1–22.

Dickinson, B.C., and Chang, C.J. (2011). Chemistry and biology of reactive oxygen species in signaling or stress responses. Nat. Chem. Biol. *7*, 504–511.

Dietrich, M.O., Liu, Z.W., and Horvath, T.L. (2013). Mitochondrial dynamics controlled by mitofusins regulate Agrp neuronal activity and diet-induced obesity. Cell *155*, 188–199.

Du Plessis, S.S., Cabler, S., McAlister, D.A., Sabanegh, E., and Agarwal, A. (2010). The effect of obesity on sperm disorders and male infertility. Nat. Rev. Urol. *7*, 153–161.

Eddy, E.M. (1975). Germ plasm and the differentiation of the germ cell line. Int. Rev. Cytol. *43*, 229–280.

Figueroa, M.E., Abdel-Wahab, O., Lu, C., Ward, P.S., Patel, J., Shih, A., Li, Y., Bhagwat, N., Vasanthakumar, A., Fernandez, H.F., et al. (2010). Leukemic IDH1 and IDH2 mutations result in a hypermethylation phenotype, disrupt TET2 function, and impair hematopoietic differentiation. Cancer Cell *18*, 553–567.

Filadi, R., Greotti, E., Turacchio, G., Luini, A., Pozzan, T., and Pizzo, P. (2015). Mitofusin 2 ablation increases endoplasmic reticulum-mitochondria coupling. Proc. Natl. Acad. Sci. U S A *112*, E2174–E2181.

Gallardo, T., Shirley, L., John, G.B., and Castrillon, D.H. (2007). Generation of a germ cell-specific mouse transgenic Cre line, Vasa-Cre. Genesis *45*, 413–417.

Gaut, J.R., and Hendershot, L.M. (1993). The modification and assembly of proteins in the endoplasmic reticulum. Curr. Opin. Cell Biol. *5*, 589–595.

Gou, L.T., Kang, J.Y., Dai, P., Wang, X., Li, F., Zhao, S., Zhang, M., Hua, M.M., Lu, Y., Zhu, Y., et al. (2017). Ubiquitination-deficient mutations in human Piwi cause male infertility by impairing histone-to-protamine exchange during spermiogenesis. Cell *169*, 1090–1104.e13.

Grivna, S.T., Beyret, E., Wang, Z., and Lin, H. (2006). A novel class of small RNAs in mouse spermatogenic cells. Genes Dev. *20*, 1709–1714.

Hofmann, M.C., Narisawa, S., Hess, R.A., and Millan, J.L. (1992). Immortalization of germ cells and somatic testicular cells using the SV40 large T antigen. Exp. Cell Res. *201*, 417–435.

Huang, H., Gao, Q., Peng, X., Choi, S.Y., Sarma, K., Ren, H., Morris, A.J., and Frohman, M.A. (2011). piRNA-associated germline nuage formation and spermatogenesis require MitoPLD profusogenic mitochondrial-surface lipid signaling. Dev. Cell *20*, 376–387.

Ikawa, M., Tergaonkar, V., Ogura, A., Ogonuki, N., Inoue, K., and Verma, I.M. (2002). Restoration of spermatogenesis by lentiviral gene transfer: offspring from infertile mice. Proc. Natl. Acad. Sci. U S A *99*, 7524–7529.

Khacho, M., Clark, A., Svoboda, D.S., Azzi, J., MacLaurin, J.G., Meghaizel, C., Sesaki, H., Lagace, D.C., Germain, M., Harper, M.E., et al. (2016). Mitochondrial dynamics impacts stem cell identity and fate decisions by regulating a nuclear transcriptional program. Cell Stem Cell *19*, 232–247.

Lau, N.C., Seto, A.G., Kim, J., Kuramochi-Miyagawa, S., Nakano, T., Bartel, D.P., and Kingston, R.E. (2006). Characterization of the piRNA complex from rat testes. Science *313*, 363–367.

Li, X., Mao, Z., Wu, M., and Xia, J. (2013). Rescuing infertility of Pick1 knockout mice by generating testis-specific transgenic mice via testicular infection. Sci. Rep. *3*, 2842.

Ma, L., Buchold, G.M., Greenbaum, M.P., Roy, A., Burns, K.H., Zhu, H., Han, D.Y., Harris, R.A., Coarfa, C., Gunaratne, P.H., et al. (2009). GASZ is essential for male meiosis and suppression of retrotransposon expression in the male germline. PLoS Genet. *5*, e1000635.

Mandal, S., Lindgren, A.G., Srivastava, A.S., Clark, A.T., and Banerjee, U. (2011). Mitochondrial function controls proliferation and early differentiation potential of embryonic stem cells. Stem Cells *29*, 486–495.

Mecklenburg, J.M., and Hermann, B.P. (2016). Mechanisms regulating spermatogonial differentiation. Results Probl. Cell Differ. *58*, 253–287.

Ramalho-Santos, J., and Amaral, S. (2013). Mitochondria and mammalian reproduction. Mol. Cell. Endocrinol. *379*, 74–84.

Rizzuto, R., Pinton, P., Carrington, W., Fay, F.S., Fogarty, K.E., Lifshitz, L.M., Tuft, R.A., and Pozzan, T. (1998). Close contacts with the endoplasmic reticulum as determinants of mitochondrial Ca^{2+} responses. Science *280*, 1763–1766.

Rovira-Llopis, S., Banuls, C., Diaz-Morales, N., Hernandez-Mijares, A., Rocha, M., and Victor, V.M. (2017). Mitochondrial dynamics in type 2 diabetes: pathophysiological implications. Redox Biol. *11*, 637–645.

Santel, A., Frank, S., Gaume, B., Herrler, M., Youle, R.J., and Fuller, M.T. (2003). Mitofusin-1 protein is a generally expressed mediator of mitochondrial fusion in mammalian cells. J. Cell Sci. *116*, 2763–2774.

Schneeberger, M., Dietrich, M.O., Sebastian, D., Imbernon, M., Castano, C., Garcia, A., Esteban, Y., Gonzalez-Franquesa, A., Rodriguez, I.C., Bortolozzi, A., et al. (2013). Mitofusin 2 in POMC neurons connects ER stress with leptin resistance and energy imbalance. Cell *155*, 172–187.

Shyh-Chang, N., Daley, G.Q., and Cantley, L.C. (2013). Stem cell metabolism in tissue development and aging. Development *140*, 2535–2547.

Son, M.J., Kwon, Y., Son, M.Y., Seol, B., Choi, H.S., Ryu, S.W., Choi, C., and Cho, Y.S. (2015). Mitofusins deficiency elicits mitochondrial metabolic reprogramming to pluripotency. Cell Death Differ. *22*, 1957–1969.

Wanet, A., Arnould, T., Najimi, M., and Renard, P. (2015). Connecting mitochondria, metabolism, and stem cell fate. Stem Cells Dev. *24*, 1957–1971.

Wang, J., Tang, C., Wang, Q., Su, J., Ni, T., Yang, W., Wang, Y., Chen, W., Liu, X., Wang, S., et al. (2017). NRF1 coordinates with DNA methylation to regulate spermatogenesis. FASEB J. *31*, 4959–4970.

Watanabe, T., Chuma, S., Yamamoto, Y., Kuramochi-Miyagawa, S., Totoki, Y., Toyoda, A., Hoki, Y., Fujiyama, A., Shibata, T., Sado, T., et al. (2011). MITOPLD is a mitochondrial protein essential for nuage formation and piRNA biogenesis in the mouse germline. Dev. Cell *20*, 364–375.

Wylie, C. (1999). Germ cells. Cell *96*, 165–174.

Yang, Q.E., and Oatley, J.M. (2014). Spermatogonial stem cell functions in physiological and pathological conditions. Curr. Top. Dev. Biol. *107*, 235–267.

Zhang, J., Wang, Q., Wang, M., Jiang, M., Wang, Y., Sun, Y., Wang, J., Xie, T., Tang, C., Tang, N., et al. (2016). GASZ and mitofusin-mediated mitochondrial functions are crucial for spermatogenesis. EMBO Rep. *17*, 220–234.

Zhou, W., Choi, M., Margineantu, D., Margaretha, L., Hesson, J., Cavanaugh, C., Blau, C.A., Horwitz, M.S., Hockenbery, D., Ware, C., et al. (2012). HIF1alpha induced switch from bivalent to exclusively glycolytic metabolism during ESC-to-EpiSC/hESC transition. EMBO J. *31*, 2103–2116.

Stem Cell Reports, Volume *14*

Supplemental Information

MFN2 Plays a Distinct Role from MFN1 in Regulating Spermatogonial Differentiation

Wei Chen, Yun Sun, Qi Sun, Jingjing Zhang, Manxi Jiang, Chingwen Chang, Xiaoli Huang, Chuanyun Wang, Pengxiang Wang, Zhaoran Zhang, Xuejin Chen, and Yuan Wang

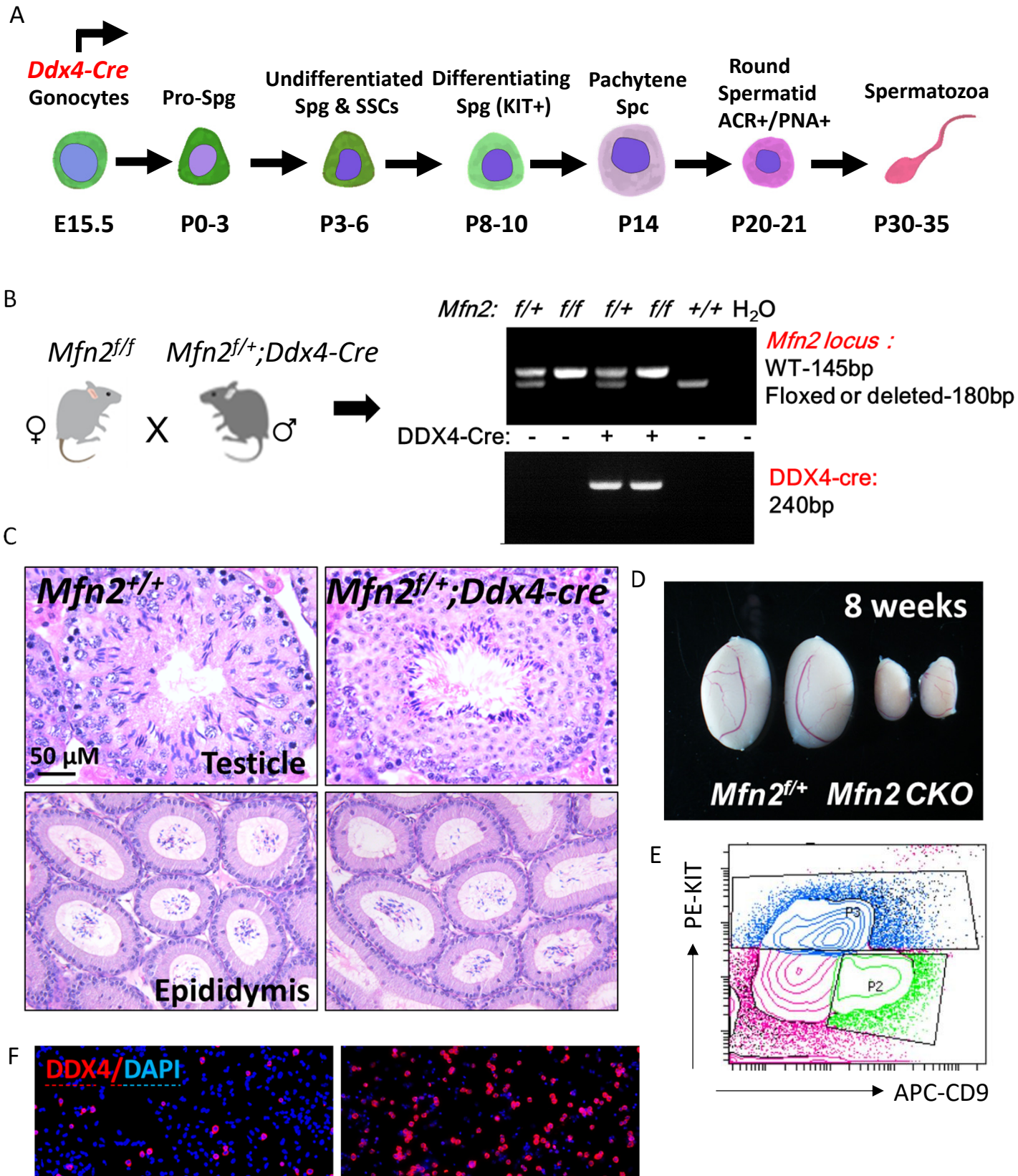

Chen et al., Supplemental Figure S1

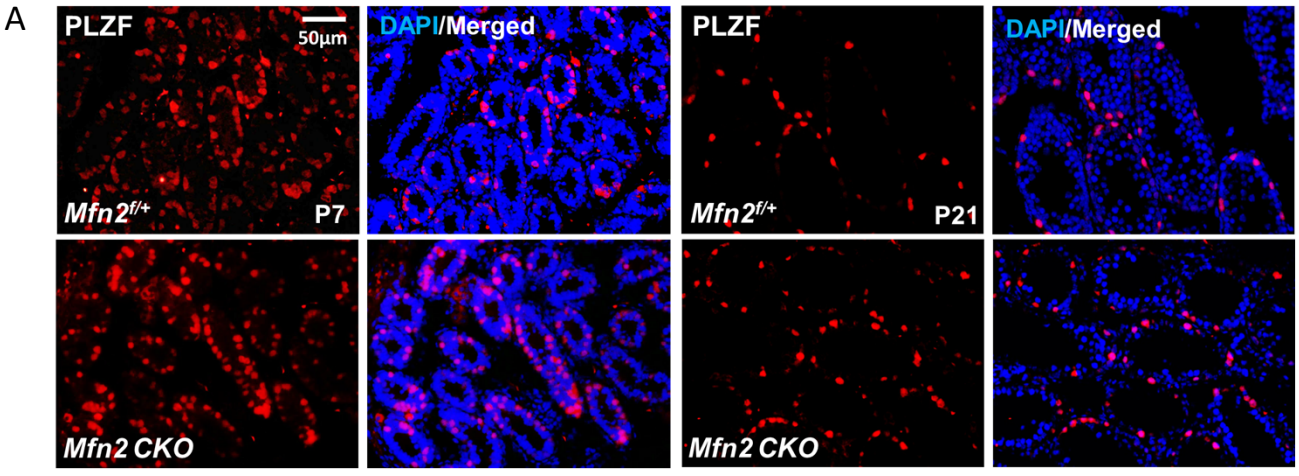

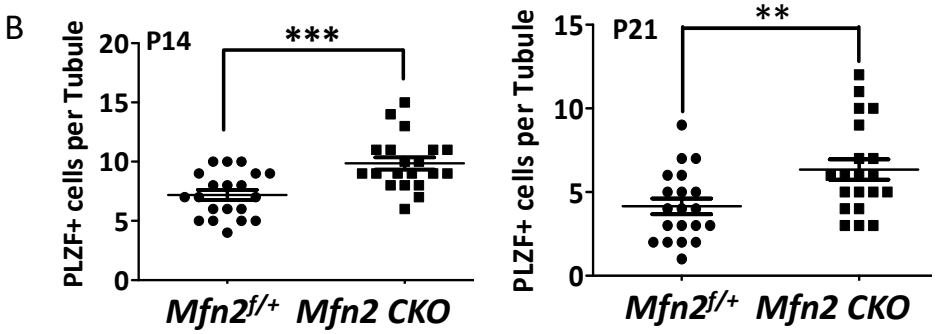

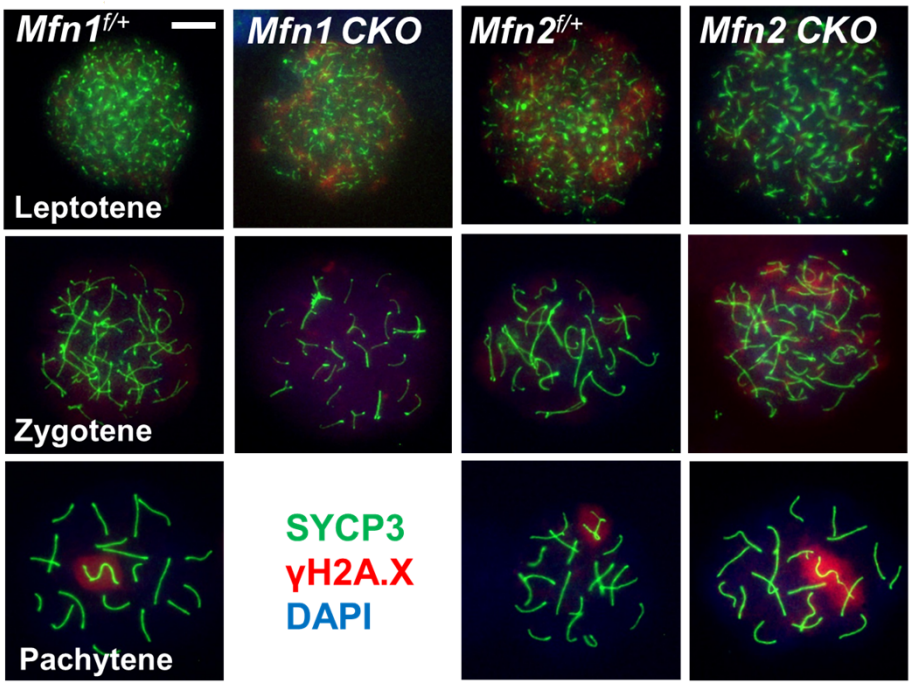

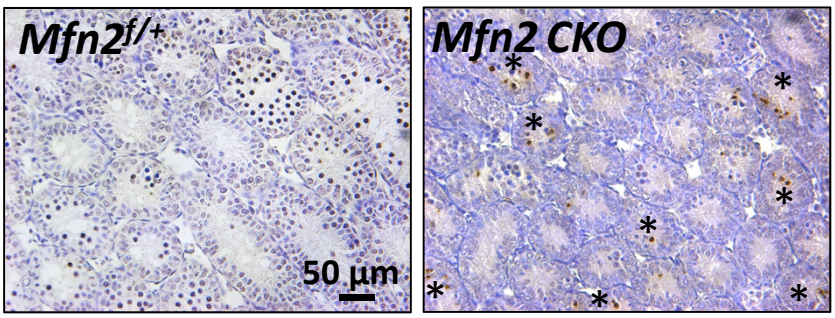

Chen et al., Supplemental Figure S2

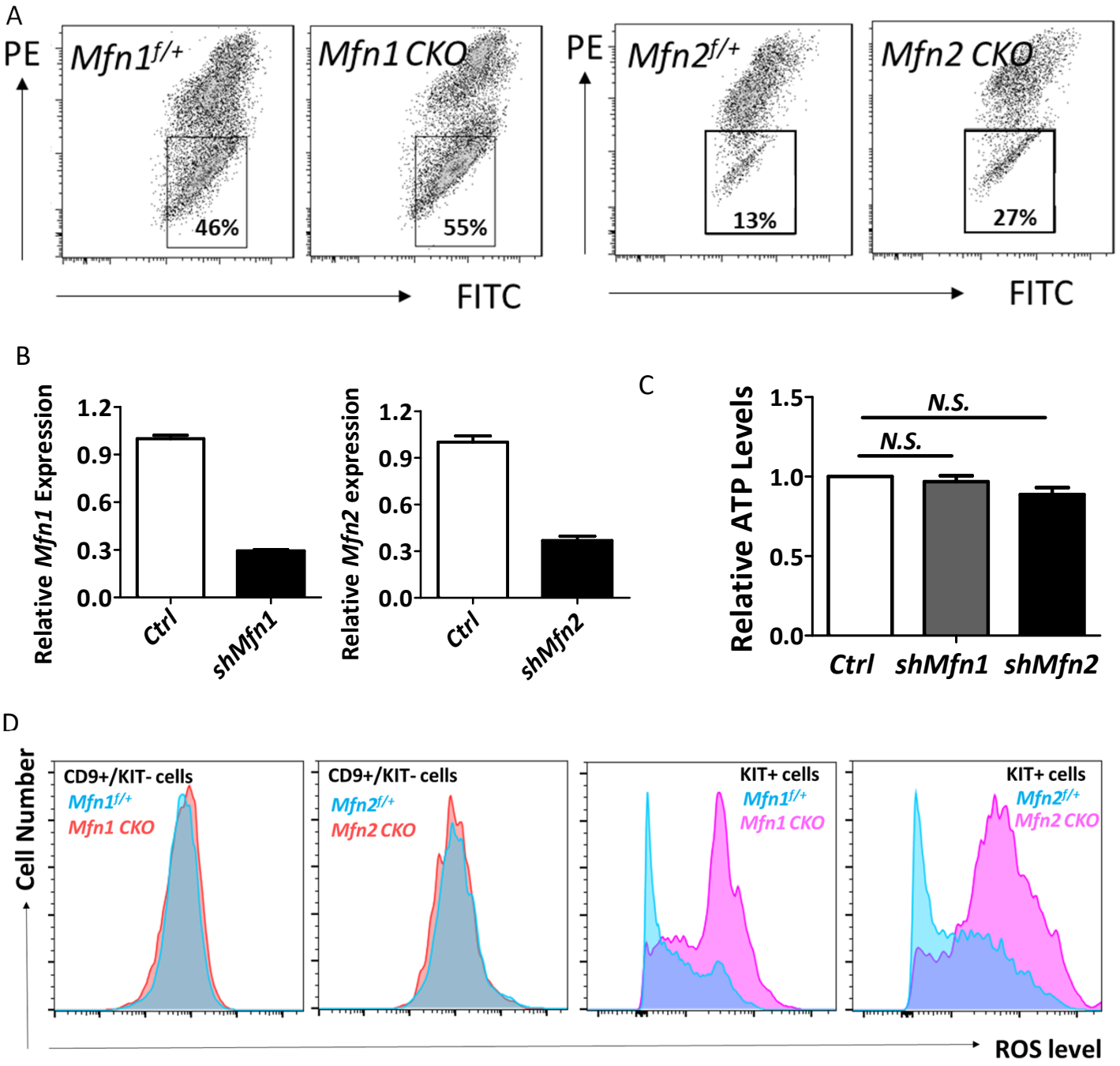

Chen et al., Supplemental Figure S3

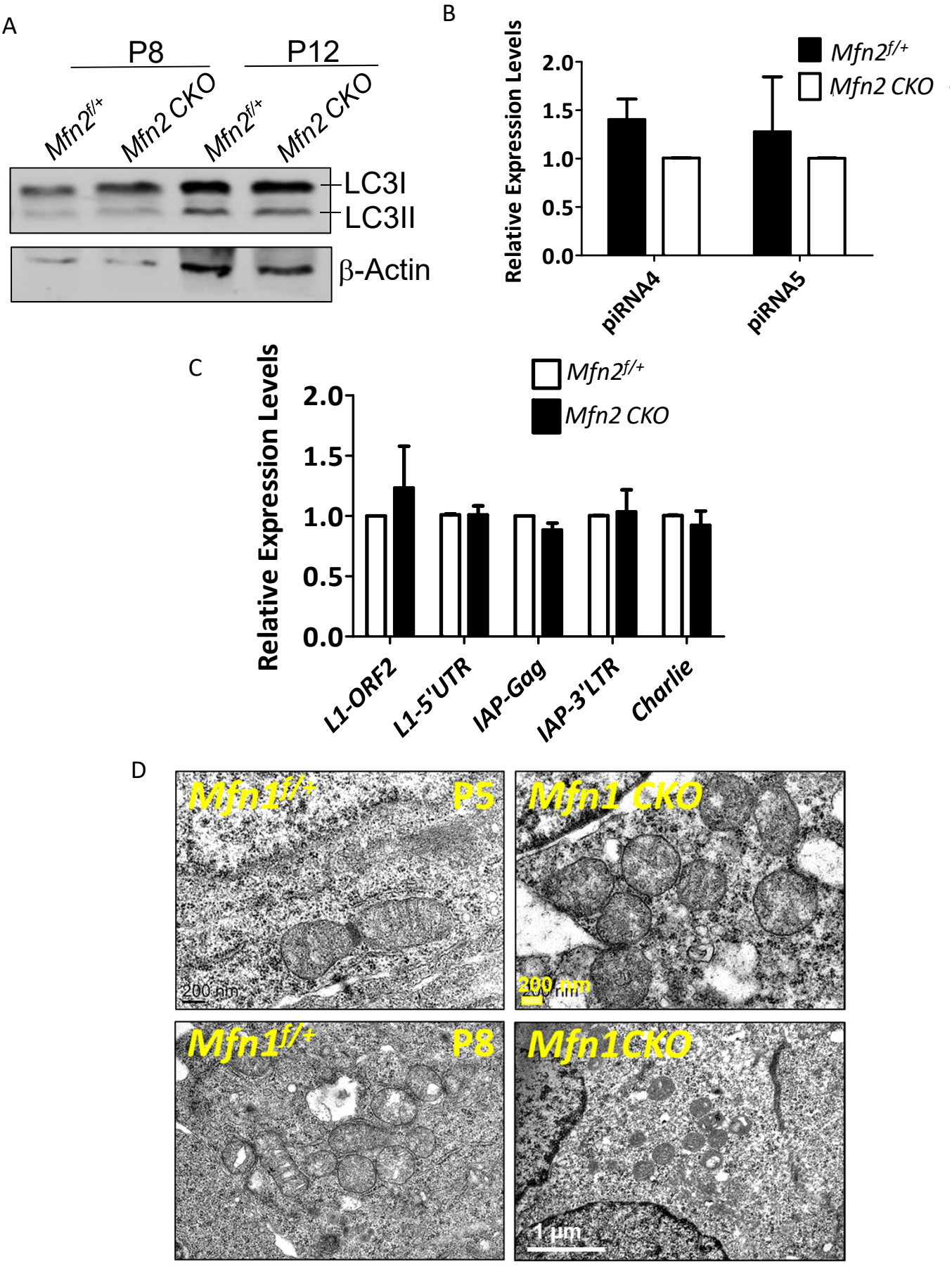

Chen et al., Supplemental Figure S4

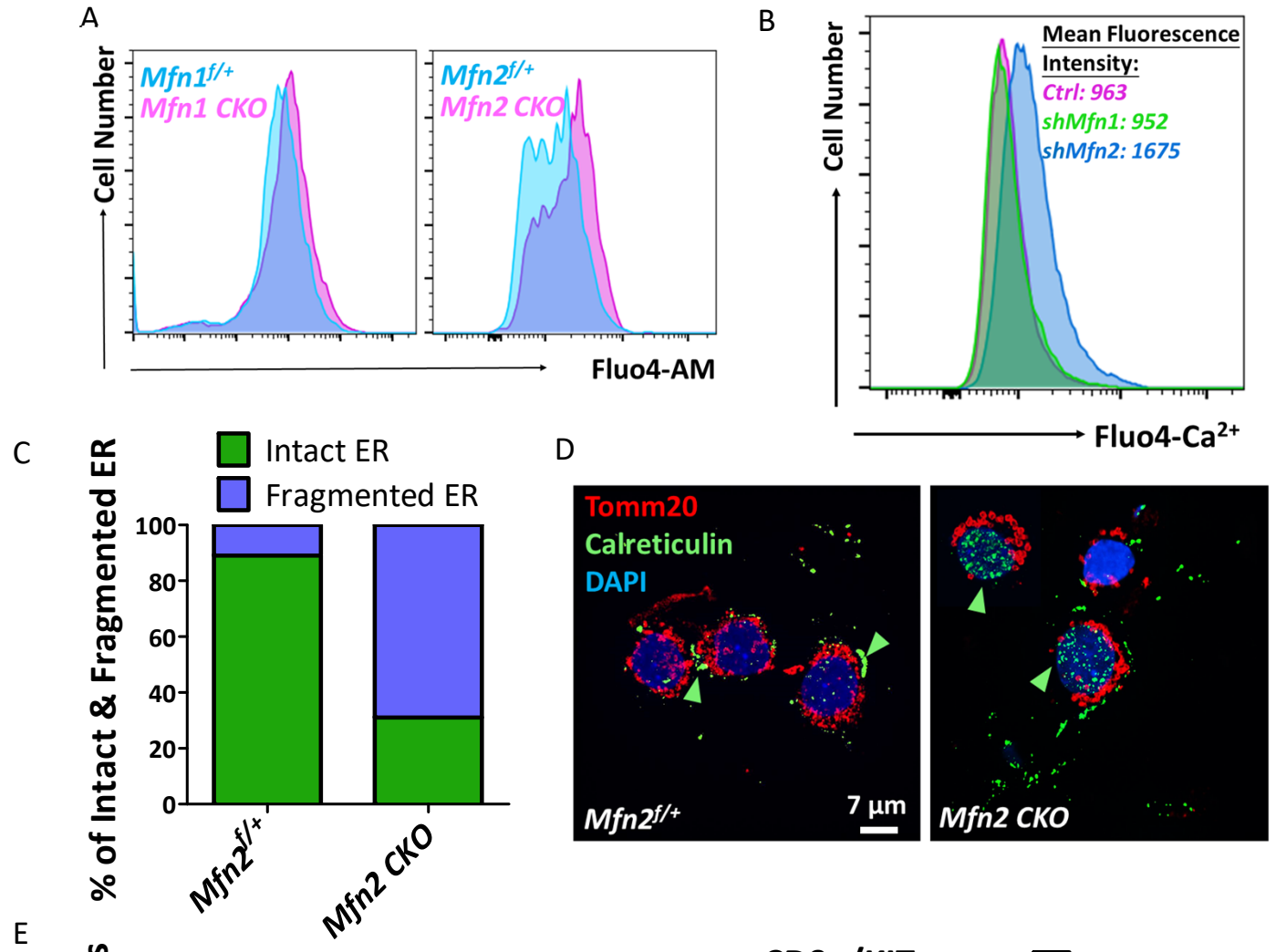

Chen et al., Supplemental Figure S5

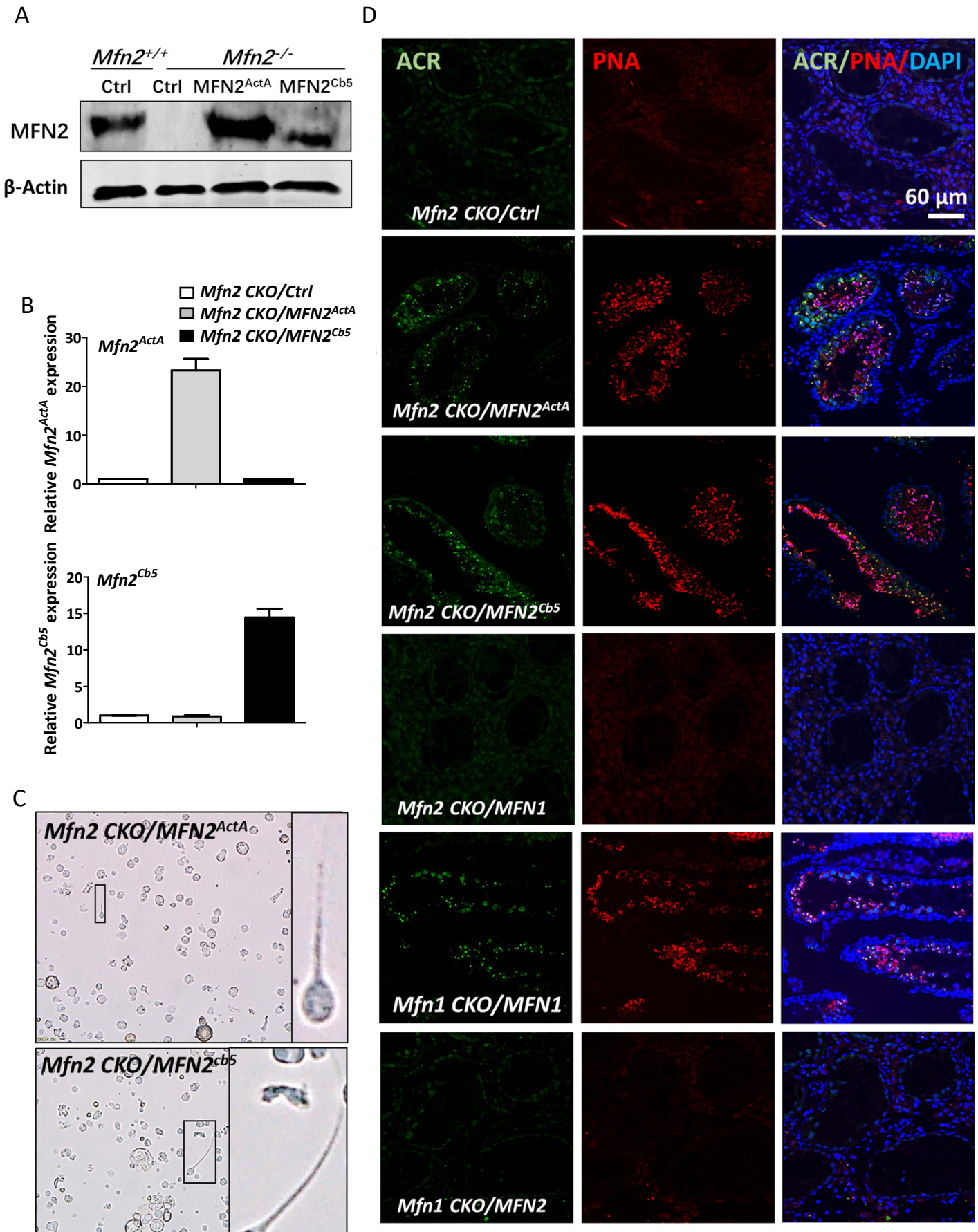

Chen et al., Supplemental Figure S6

Supplemental Figure Legends

Fig. S1. Charactering MFN deficient testes. (**A**) Timeline of male germ cell development in mice. Differentiating spermatogonia start to appear at P8-10, with pachytene spermatocytes at P14, and haploid spermatid around P21. Therefore, in our study, we assessed undifferentiated and differentiating spermatogonia between P10-12, performed meiosis chromosome spreading assay to detect primary spermatocytes at P14, and examined testes with viral introduction at 30-40 days post injection to detect haploid spermatid formation from spermatogonia. (**B**) Breeding and genotyping strategies to obtain *Mfn2*$^{f/+}$ mice and *Mfn2*$^{f/f}$*; Ddx4-Cre* littermates. (**C**) Histological studies of testis and epididymis sections from wild-type adult mice or mice with heterozygote *Mfn2* deletion in germ cells. No obvious alteration in male reproductive organs was observed in mice with heterozygote *Mfn2* deletion in germ cells. (**D**) Gross morphology of testes from *Mfn2*$^{f/+}$ or *Mfn2*$^{f/f}$*; Ddx4-Cre* adult mice at 8 weeks. (**E**) An example of CD9 and KIT staining analyzed by flow cytometry. (**F**) An example of IF with DDX4 antibody to assess the percentage of germ cells collected using serial adhering procedures. Dissociated germ cells are loosely attached to the tissue culture plates compared to somatic and supporting cells which are tightly adhered to the plates. Using serial adhering procedures, the germ cells can be lifted easily and separated from somatic cells. The percentage of DDX4+ cells was ~8% in dissociated single cell population from testes (Before) and increased to >75% after serial adhering procedures (After).

Fig. S2. *Mfn2* conditional knockout in germ cells specifically impairs differentiating spermatogonia and spermatocytes. (**A**) IHF on testicle sections from *Mfn2*$^{f/+}$ or *Mfn2*$^{f/f}$*; Ddx4-Cre* mice at P7 and P21 with an antibody against PLZF. (**B**) Numbers of PLZF+ spermatogonia per seminiferous tubule section from *Mfn2*$^{f/+}$ and *Mfn2*$^{f/f}$*; Ddx4-Cre* mice at P7 and P21. Data are presented as mean ± one s.e.m. **: $P<0.01$; ***: $P<0.001$. (**C**) Meiosis chromosome spreading was performed on P14 testes with *Mfn1* or *Mfn2* conditional deletion in germ cells and those from their

littermate controls. The prophase I of primary spermatocytes was staged according to co-staining of SYCP3 with γ-H2A.X. (**D**) Apoptosis was examined by TUNEL assays on testis sections from *Mfn2*$^{f/+}$ and *Mfn2*$^{f/f}$*; Ddx4-Cre* mice at P14. The seminiferous tubules with brown apoptotic cells were labeled with *.

Fig. S3. MFN deficiency compromises mitochondrial functions in differentiating spermatogonia and spermatocytes. (**A**) Examples of flow cytometry analyses to examine mitochondrial membrane potential of non-adherent germ cells collected from mice at P12. (**B**) *Mfn1* and *Mfn2* transcript levels were analyzed by real-time RT-PCR upon shRNA knockdown of MFN1 and MFN2 respectively. (**C**) ATP levels were measured on GC1 cells infected with scrambled shRNA (*Ctrl*), shRNAs against MFN1 or MFN2 (shMfn1 or shMfn2). Relative ATP levels were calculated in comparison to scrambled shRNA control. (**D**) Examples of flow cytometry analyses to examine ROS levels in germ cells sorted from mice at P12.

Fig. S4. MFN deficiency does not affect autophagy or the expression of piRNA and transposable elements in germ cells. (**A**) Autophagy was examined by measuring LC3I/II ratio with Western Blotting on *Mfns*$^{f/+}$ and *Mfn2*$^{f/f}$*; Ddx4-Cre* testes at P12. (**B-C**) Expression levels of piRNAs (**B**) and transposable elements (**C**) were measured with real-time RT-PCR assays on *Mfn2*$^{f/+}$ and *Mfn2*$^{f/f}$*; Ddx4-Cre* P4 testes. (**B-C**) Data are presented as mean ± one s.e.m. N=3. No statistically significant difference in their expression levels between *Mfn2*$^{f/+}$ and *Mfn2*$^{f/f}$*; Ddx4-Cre* groups was observed. (**D**) Mitochondrial architecture was examined by TEM on testicle sections from control or *Mfn1* conditional knockout mice at P5 and P8. Fragmented and small mitochondria were observed in *Mfn1* knockout testes at P8.

Fig. S5. Deletion of *Mfn2* but not *Mfn1* leads to disturbed ER functions in germ cells. (**A**) An example of flow cytometry to measure Ca^{2+} levels (Fluo-3 AM intensity) in non-adherent germ cells collected from testes of P12 mice. (**B**) Ca^{2+} levels were measured in GC1 cells with scrambled shRNA (Ctrl) or shRNA against MFN1 or

MFN2. Mean Fluo-4 AM intensity from each group was shown. (**C**) The percentages of *Mfn2*$^{f/+}$ and *Mfn2*$^{f/f}$*; Ddx4-Cre* germ cells with intact ER or fragmented ER detected by TEM were calculated from 9-13 sample grids. (**D**) 3-D super-resolution imaging with Tomm 20 and Calreticulin co-staining was performed on *Mfn2*$^{f/+}$ and *Mfn2*$^{f/f}$*; Ddx4-Cre* germ cells. Green arrows point to ER. Swollen mitochondria and fragmented ER with increased Calreticulin expression were observed in *Mfn2*$^{f/f}$*; Ddx4-Cre* germ cells. (**E**) Transcript levels of ER chaperons were measured by real-time RT-PCR on non-adherent germ cells (left panel) or CD9+/KIT- spermatogonia (right panel) from P12 *Mfn2*$^{f/+}$ and *Mfn2*$^{f/f}$*; Ddx4-Cre* mice. Data are presented as mean ± one s.e.m. from three biological replicates. *: $P<0.05$. **: $P<0.01$. (**F**) Calreticulin expression was examined by Western Blots on GC1 cells with scrambled shRNA (Ctrl), shRNA against MFN1 or MFN2.

Fig. S6. MFN2 plays a non-redundant role in germ cell development from MFN1. (**A**) MFN2 expression was examined by Western Blots on wild-type or *Mfn2*$^{-/-}$ MEFs infected with empty vector control viruses (Ctrl) or viruses expressing MFN2 tagged with mitochondrion (MFN2^{ActA})- or ER (MFN2^{Cb5})-localization signaling peptides. β-actin served as a loading control. (**B**) Expression of MFN2^{ActA} or MFN2^{Cb5} were detected by real-time RT-PCR in non-adherent germ cells from *Mfn2*$^{f/f}$*; Ddx4-Cre* mice rescued with control viruses (Ctrl) or viruses expressing MFN2^{ActA} or MFN2^{Cb5} at day 40 post infection. Data are presented as mean ± one s.e.m. from three independent experiments. (**C**) Fully developed spermatozoa were detected in dissociated cells from *Mfn2*$^{f/f}$*; Ddx4-Cre* testes infected with viruses expressing MFN2^{ActA} or MFN2^{Cb5} at day 40 post injection. (**D**) IHF analyses with an antibody against acrosin (ACR) and stained with peanut agglutinin (PNA), counterstained with DAPI, on testis sections from mice at day 40 post viral infection with ActA- or Cb5-tagged MFN2, full-length MFN1, or MFN2 through seminiferous tubules. Ctrl: control virus produced with an empty vector.

	Supplemental Table S1 Primers used in this study
Primers for genotyping	
Primer Name	**Sequences (5'-3')**
Mfn1 or Mfn2 conditional knockout mice	
Mfn1-genotyping-F	TTGGTAATCTTTAGCGGTGCTC
Mfn1-genotyping-R	AGCAGTTGGTTGTGTGACCA
Mfn1-genotyping-exc-R	TTAAAGACACGGCTAATGGCAG
Mfn2-genotyping-F	GAAGTAGGCAGTCTCCATCG
Mfn2-genotyping-R	AACATCGCTCAGCCTGAACC
Ddx4-cre Mouse	
Transgene _MVH-Cre_For	CACGTGCAGCCGTTTAAGCCGCGT
Transgene _MVH-Cre_Rev	TTCCCATTCTAAACAACACCCTGAA
Primers for real-time PCR (mRNA and tranposons)	
Primer Name	**Sequences (5'-3')**
m-RT-Mfn1-F	ATGGCAGAAACGGTATCTCCA
m-RT-Mfn1-R	CTCGGATGCTATTCGATCAAGTT
m-RT-Mfn2-F	GTGGGCTGGAGACTCATCG
m-RT-Mfn2-R	CTCACTGGCGTATTCCACAA
M-RT-Grp78-F	ACTTGGGGACCACCTATTCCT
M-RT-Grp78-R	ATCGCCAATCAGACGCTCC
M-RT-Grp94-F	TCGTCAGAGCTGATGATGAAGT
M-RT-Grp94-R	GCGTTTAACCCATCCAACTGAAT
M-RT-Grp75-F	ATGGCTGGAATGGCCTTAGC
M-RT-Grp75-R	ACCCAAATCAATACCAACCACTG
M-RT-ATF4-F	AAGGAGGAAGACACTCCCTCT
M-RT-ATF4-R	CAGGTGGGTCATAAGGTTTGG
M-RT-Bip-F	ACTTGGGGACCACCTATTCCT
M-RT-Bip-R	ATCGCCAATCAGACGCTCC
M-RT-CHOP-F	CTGGAAGCCTGGTATGAGGAT
M-RT-CHOP-R	CAGGGTCAAGAGTAGTGAAGGT
M-RT-Xbp1-F	GACAGAGAGTCAAACTAACGTGG
M-RT-Xbp1-R	GTCCAGCAGGCAAGAAGGT
M-RT-Mfn2-ActA/Cb5-F	CCAGCAAGTTGACATCACCCG
M-RT-Mfn2-ActA-R	GATAAACGCCCCTAAAGAGAA
M-RT-Mfn2-Cb5-R	CAGGGCTGAGATGGCTGGGAT
M-RT-β-Actin-F	GGCTGTATTCCCCTCCATCG
M-RT-β-Actin-R	CCAGTTGGTAACAATGCCATGT
L1-ORF2-Q-F	GGAGGGACATTTCATTCTCATCA
L1-ORF2-Q-R	GCTGCTCTTGTATTTGGAGCATAGA
L1-5'UTR-Q-F	GGCGAAAGGCAAACGTAAGA

L1-5'UTR-Q-R	GGAGTGCTGCGTTCTGATGA
IAP-Gag-Q-F	AACCAATGCTAATTTCACCTTGGT
IAP-Gag-Q-R	GCCAATCAGCAGGCGTTAGT
IAP-3'LTR-Q-F	GCACATGCGCAGATTATTTGTT
IAP-3'LTR-Q-R	CCACATTCGCCGTTACAAGAT
Charlie-Q-F	TTGAGAATCGGATGGGAGAC
Charlie-Q-R	AAGAACTGTCTTATTCAGGC
Primers for real-time RT-PCR of 5S rRNA and piRNAs	
Primer Name	**Sequences (5'-3')**
5S-RT	CTCAACTGGTGTCGTGGAGTCGGCAATTCAGTTGAGAAAGCCTA
5S- Forward	ACACTCCAGCTGGGGCCTGGGAATACCGG
Universal-QPCR-Rev	CTCAACTGGTGTCGTGGAGTCGG
piRNA4-RT	CTCAACTGGTGTCGTGGAGTCGGCAATTCAGTTGAGCTTCGTCTCCG
piRNA4-OPCR-Forward	ACACTCCAGCTGGGGTAATCCCAGCTCTTGG
piRNA5-RT	CTCAACTGGTGTCGTGGAGTCGGCAATTCAGTTGAGTCCCAAACA
piRNA5-Forward	ACACTCCAGCTGGGGTCAGCCCTCGACACA
Primers for cloning shRNAs	
m-Mfn1-shRNA-F	CCGGCCCAGTGTACTGAAAGTGTATCTCGAGATACACTTTCAGTACACTGGGTTTTTG
m-Mfn1-shRNA-R	AATTCAAAAACCCAGTGTACTGAAAGTGTATCTCGAGATACACTTTCAGTACACTGGG
m-Mfn2-shRNA-F	TGCTGGACAGCTGGATTGATAATTCAAGAGATTATCAATCCAGCTGTCCAGCTTTTTTC
m-Mfn2-shRNA -R	TCGAGAAAAAAGCTGGACAGCTGGATTGATAATCTCTTGAATTATCAATCCAGCTGTCCAGCA
Scramble-sense	TGAGCGTGTAGTCACGCATAGCCCTGACCCAGCTATGCGTGACTACACGCTCTTTTTC
Scramble-antisense	TCGAGAAAAAGAGCGTGTAGTCACGCATAGCTGGGTCAGGGCTATGCGTGACTACACGCTCA

Supplemental Experimental Procedures and Materials

Cell Culture

GC1 (ATCC, CRL-2053), *Mfn2*$^{+/+}$ and *Mfn2*$^{-/-}$ MEFs (kind gifts from Dr. Quan Chen, Institute of Physics, Chinese Academy of Sciences), and 293T cells were maintained in DMEM/10% FBS (Fetal Bovine Serum, Sigma-Aldrich). Viruses were produced using

293T cells following standard procedures.

Collecting germ cells using serial adhering procedures, Immunofluorescence (IF) Assays, and 3D super-resolution imaging

Testes were mechanically disassembled into small pieces and incubated sequentially in 1 mg/ml collagenase IV/PBS (Thermo Fisher Scientific, 17104019) for 15 min and 0.05% trypsin/PBS (Thermo Fisher Scientific, 25200072) for 5 min with occasional agitation. Dissociated single cells were sequentially plated onto gelatin-coated plates with DMEM/10% FBS in 37°C/5% CO_2 incubator for ~1 hr and 3 hr. Non-adherent cells were carefully collected from supernatant and plated onto Matrigel (Corning, 354234)-coated glass slide or plates. For IF assays, cells were fixed in 4% paraformaldehyde after plating onto Matrigel for 4 hr, followed by staining with primary and fluorochrome-conjugated secondary antibodies. For other assays, after 1-2 hr incubation on Matrigel, loosely adherent germ cells were collected by gently pipetting and lifting them from residue tightly adherent somatic/supporting cells. IF was performed using the following antibodies, probes, or fluorescent dyes: 8-Oxoguanine (Merck Millipore, MAB3560-C), MitoTracker (Thermo Fisher Scientific, M22425), Fluo3-AM (S1056) and Hoechst 33342 (C1022) from Beyotime Biotechnology (Shanghai, China), Tomm 20 (Abcam, ab186735), Calreticulin (BD Biosciences, 612137). Alexa Fluor 488- or TRITC-conjugated anti-mouse, or anti-rabbit secondary antibodies are from Jackson ImmunoResearch. Images were obtained using a Leica confocal microscope. The 3D super-resolution imaging was performed using a high speed Andor dragonfly confocal platform (Oxford Instruments Company, Unite Kingdom).

Meiotic Chromosome Spreading Assays

Dissociated germ cells were incubated in hypo-extraction buffer (30 mM Tris, 50 mM Sucrose, 17 mM NaCitrate, 5 mM EDTA, pH 8.3) and Protease Inhibitor Cocktail (Santa Cruz Biotech) on ice for 90 min. Cells were then resuspended in 20 µl hypo-extraction buffer with 60 µl 100 mM sucrose, cytospined onto slide, fixed in 4 % PFA

for 15 min, and incubated with 0.04 % photoflo (KODAK) for 5 min. Air dried slides were blocked with 3% BSA/PBS for 30 min at room temperature and stained with SYCP3 (Abcam, ab15093) and γ-H2A.X (Merck Millipore, 05-636) antibodies at 4ºC and fluorescence-conjugated secondary antibodies (Jackson ImmunoResearch) with DAPI afterwards. Images were captured under a Leica microscope with oil immersion lens.

TUNEL assays

Mouse testes were fixed in 4% PFA in PBS at 4°C overnight and were embedded in paraffin. Testicle sections were digested with 20 μg/ml protease K at room temperature for 20 minutes before staining for apoptotic cells with a DeadEnd™ Colorimetric TUNEL System (VWR/Promega, PAG3250/G3250) following the manufacturer's instruction.

Measurement of ATP Levels

Cellular ATP levels were measured using an ATP Assay Kit (Beyotime Biotech， S0026) according to manufacturer's instructions. Briefly, dissociated germ cells were lysed and centrifuged at 12,000 rpm for 5 min. Supernatants (60 μL) were mixed with 60 μL of ATP detection buffer in a 96-well plate. Luminance (RLU) was measured using an Infinite™ M200 Microplate Reader (Thermo Fisher Scientific). Protein concentration for each sample was determined by Bradford protein assay, and ATP concentration (μM) per mg of protein was calculated. Three or more technical replicates were examined for each independent experiment.

Western Blots

Western blots were performed according to standard protocols and the final fluorescent signals against targeted proteins were detected using the Li-COR Odyssey system (LI-COR Biosciences). Primary antibodies used in this study: MFN1 (Absci, AB45059), MFN2 (Abcam, ab189862), β-Actin (Santa Cruz Biotech, sc-10731), Bip/GRP78

(Santa Cruz Biotech, 610978), CHOP (Santa Cruz Biotech, SC793), Calreticulin (BD Biosciences, 612137). For autophagy detection by Western Blotting, an antibody against LC3B from Sigma-Aldrich (L7543) was used to detect LC3B-I (18kDa) and LC3B-II (16kDa) with Western blotting analyses according to standard protocols.

Determination of the Expression Levels of piRNA

Total RNAs were extracted from testes using Trizol according to Manufacturer's instructions with a minor modification in the RNA precipitation step. Briefly, samples with isopropanol was centrifuged at 4℃ 12,000 rpm for a prolonged time (40 min) to ensure efficient precipitation of small size RNAs. Reverse transcription was carried out using PrimeScript® RT Kit with gDNA Eraser (Takara) and piRNA specific RT primers. Quantitative real-time PCR was performed on Stratagene MX3000P instrument using SYBR Premix Ex TaqTM II (Takara). The expression levels of piRNA were normalized to 5S rRNA. Primers used in this study were listed in Supplemental Table S1.

Construction of Knockdown Plasmids

The shRNA against *Mfn1* was cloned into *pLKO.1-puro* vector. The *Mfn2* shRNA and a scramble shRNA control were designed and cloned into pll3.7-U6-MCS-EF1α-EGFP vector. Inserted shRNA sequences were confirmed by DNA sequencing. The shRNA sequences were provided in Supplemental Table S1.